Utrecht University

# REGIONAL SEA LEVEL ALLOWANCES ALONG THE WORLD COAST-LINE

**MASTER'S THESIS**

**CHRISTOS TSITSIKAS**

DECEMBER 2017

**Project Supervisor**:
Dr. Roderik van de Wal

**Second Examiner:**
Dr. C. H. Reijmer-Tijm

# Abstract

Sea level changes as a result of climate change. For projections we take ocean mass changes and volume changes into account. Including gravitational and rotational fingerprints these provide regional sea level changes. Hence, we can calculate sea-level rise patterns based on Coupled Model Intercomparison Project Phase 5 (CMIP5) projections. The variability around the mean state,originating from the climate models, is taken into account by using the concept of allowances. An allowance is the height by which a coastal infrastructure must increase in order to retain the same risk of flooding events occurring due to climate change. It is computed by taking in account the mean and uncertainty of sea level change projections, as well as the variability of extreme sea levels caused by i.e. tides and waves. Existing sets of allowances are based on tide gauges data records, which are spatially limited. Here we used data from a hydrodynamical model, including variability caused by tides and storm surges. Results show the need for more than 1 meter-allowances for most of coastline, with an increasing trend towards the equator. As a second step, changes in global significant wave height maxima towards the end of the century are computed and implemented. This leads to an increase of allowances mostly in high latitude ocean locations. Moreover, in the case of not including allowances in their coastal infrastructure, more than 70% of the studied locations worldwide will be strongly affected by a large increase in their flooding frequency.

**Keywords: allowance, sea level change, tides, surges, GTSR, significant wave height**

# Table of Contents

## Common Abbreviations

- CMIP5 - Coupled Model Intercomparison Project Phase 5
- GESLA-2 - Global Extreme Sea Level Analysis, Version 2
- GTSR - Global Tide and Surge Reanalysis
- IPCC - Intergovernmental Panel on Climate Change
- EAIS - East Antarctic Ice Sheet
- WAIS - Wast Antarctic Ice Sheet
- AIS - Antarctic Ice Sheet
- GIS - Greenland Ice Sheet
- SLC - Sea Level Change
- PDF - Probability Density Function

Chapter 1

# Introduction

Flooding is defined as the inundation of land by water, occurring when its level exceeds the height of coastal structure. Flooding events usually have a vast social and financial cost. A way to identify the frequency of such events is to use data records and calculate the number of exceedances of a certain level. Thus, we can have for example an 1 per 100 years exceedance frequency for a water level of i.e. 2 meters at a specific location.

This frequency will unavoidably be affected by the Sea Level Change due to climate change. This contribution has to be quantified in order to update the current coastal infrastructure. A way to do this is by computing and using allowances (Hunter, 2012), the extra height by which to raise the infrastructure in order to maintain the frequency of exceedance events at some point in the future (1.1). This takes in account the mean Sea Level Change, its uncertainty occurring from the deviations among the models, and the variability of extreme waters at each specific point. Previous work on computing a global set of allowances (Hunter et al., 2013; Slangen et al., 2017) has been done using data records from tide gauge locations along with Sea Level Change projections, leading to a total of 652 points globally.

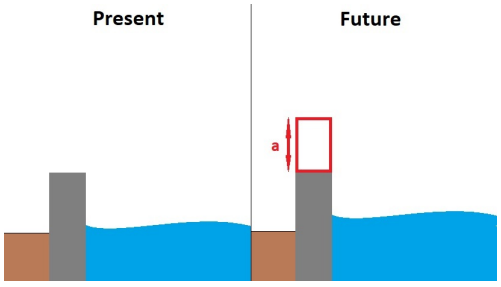


**Figure 1.1:** The additional allowance, a, for the coastal infrastructure used to maintain the same exceedance frequency after a future Sea Level Change.

The primary objective of this Master's thesis is to expand the previous allowances applications. This is done in two ways. First, the use of reanalysis data instead of the limited tide gauge records can extend the produced grid of allowances to several thousands of points. Here we use the output of a model that covers most part of the global coastline, includes both tide and storm surges, and is validated against measurement records (Muis et al., 2016).

To check the model's behavior, a comparison is made with the tide gauge records used in previous studies of allowances (chapter 3). Then, using the latest Sea Level Change projections, along

with a set of ice dynamics, a global set of allowances is computed (chapter 4). The set is also compared to the one by Slangen et al. (2017) using the same Sea Level Change projections. This leads to conclusions about climate-change influencing both the extent and magnitude of future flooding frequency.

Moreover, every approach until now has been made under the assumption that extreme sea level statistics will not change in time, as the change in frequency of flooding events is mostly connected to the mean sea level change (Menéndez and Woodworth, 2010). Here, an effort is made to include the effect of the change in wave height maxima towards the end of the century (chapter 5). This is done by using historical and end century significant wave height projections to quantify this change in the form of a skewed distribution. This way we can identify areas with increase or decrease in the peak value of the maximum wave height, as also the variability of this change. Finally, the distribution has to be included in an allowance as a change in both the mean state and the variability and thus the computation has to be altered. The result is a set of allowances that covers the effects of tides, storm surges and wave height extreme changes, which gives a more complete picture of the coastal safety situation at the end of the century.

Chapter 2

# Theory - Data - Methods

## 2.1 Theory

### 2.1.1 Allowances

Hunter (2012) describes an allowance in terms of sea level change as "the amount by which something, such as the height of coastal infrastructure, needs to be altered to cope with climate change". In order to calculate the allowance we need a sea level change projection with mean value $\mu_{SLC}$ and uncertainty $\sigma_{SLC}$. This is combined with the variability of sea level extremes, caused for example by tides or storm surges. A necessary assumption is that this variability of the extremes remains constant over time and that the mode of their distribution is zero relative to the mean sea level change (Menéndez and Woodworth, 2010). Then, the probability of no exceedances during a certain time period is

$$F = \exp(-N) \tag{2.1}$$

where N is the number of expected exceedances during the same period. To derive an analytical expression for the allowance, a specific distribution has to be chosen. For the previously computed global sets of allowances mentioned in the introduction, Gumbel distribution was used, a subcategory of the Generalised Extreme Value Distribution.

### 2.1.2 Generalised Extreme Value Distribution

The Generalised Extreme Value distribution is a group of distributions, often used for describing maxima, or minima, events. The general form of the probability density function (PDF) is:

$$\frac{1}{\lambda} t(x)^{\xi+1} e^{-t(x)} \tag{2.2}$$

where

$$t(x) = \begin{cases} (1 + \xi(\frac{x-\mu}{\lambda}))^{-\frac{1}{\xi}} & \text{if } \xi \neq 0 \\ e^{\frac{-(x-\mu)}{\lambda}} & \text{if } \xi = 0 \end{cases}$$

Parameters $\mu$, $\lambda$ and $\xi$ are called the location, scale and shape parameter respectively. Location parameter is related to the mode of the distribution, scale parameter to the variance and shape parameter to the behavior of the distribution tail. The scale parameter $\lambda$ is always positive. In the specific case

where $\xi = 0$ the resulting distribution is called the Gumbel distribution. Then, the PDF (Figure 2.1) becomes

$$\frac{1}{\lambda} e^{-(\frac{x-\mu}{\lambda} + e^{\frac{x-\mu}{\lambda}})} \tag{2.3}$$

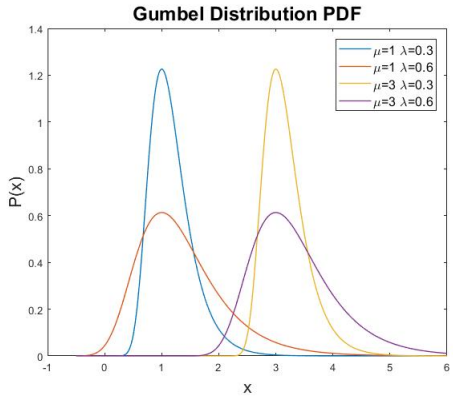


**Figure 2.1:** The Probability Density Function of a Gumbel distribution for four cases with changing location and scale parameters $\mu$ and $\lambda$.

In the case of a Gumbel distribution, location parameter represents the mode. Moreover, the mean and variance of a Gumbel distribution can be determined by the location and scale parameters as:

$$\bar{x} = \mu + \gamma\lambda \tag{2.4}$$

where $\gamma = 0.5772$ is the Euler–Mascheroni constant, and

$$\sigma^2 = \frac{\pi^2\lambda^2}{6} \tag{2.5}$$

Thus, mean and variance of a Gumbel distribution are always higher than the location and scale parameters respectively.

## 2.2 Data

### 2.2.1 Regional Sea Level Change projections

Slangen et al. (2014) computes a global grid, with a resolution of 1 degree, of regional sea level projections for the period 2010-2100. This is done by using the output of 21 CMIP5 models as their ensemble mean based on changes in ocean circulation, heat uptake and sea-level pressure. This output is combined with an ice dynamics contribution consisting of land ice, groundwater depletion and Glacial Isostatic Adjustment contributions. For this project, the set of projections for the RCP 8.5 scenario will be used, replacing the ice dynamics from Slangen et al. (2014) with the one from the IPCC scenario (Church et al., 2013). This scenario assumes a normal distribution for the ice sheet dynamical contributions for the Antarctic and Greenland ice sheets as presented in IPCC AR5. As these contributions refer to the change from the period 1986–2005 to 2081–2100, the values include a linear correction made by Slangen et al. (2017) for estimating the change for the period 2010-2100. For better accuracy, the contribution of Antarctica is split into one for the East Antarctic Ice Sheet and one for the West Antarctic Ice Sheet as has been done by Shepherd et al. (2012).

### 2.2.2 Extreme waters caused by tide and storm surges

As mentioned in section 2.1.1, additionally to Sea Level Change projections, extreme waters statistics are necessary to compute allowances. Slangen et al. (2017) used data from the Global Extreme Sea Level Analysis, version 2 dataset. For this project, extreme waters statistics are obtained from the Global Tide and Surge Reanalysis. Both datasets are presented below.

#### Global Extreme Sea Level Analysis, Version 2 (GESLA-2)

The GESLA-2 dataset consists of high frequency, per hour or less, records from 1355 tide gauge sites (Woodworth et al., 2017). The length of the records varies between 1 and 167 years. Hunter et al. (2017) fitted Gumbel distributions to these records. Slangen et al. (2014) used 652 sites from the GESLA-2 dataset using a limit of at least 30 years of data and excluding four sites with non-Gumbel behavior and two sites where no Sea Level Change data was available. Combining this data with Sea Level Change projections and ice dynamics, a set of allowances was computed for these 652 points.

#### Global Tide and Surge Reanalysis (GTSR)

The GTSR dataset describes modeled extreme water levels caused by tide and storm surges. It was created Muis et al. (2016) and covers almost the entire global coastline using an irregular grid. The Global Tide and Surge Model is used, forced with data from ERA-Interim reanalysis for atmospheric pressure and wind. The tide modeling is done by the Finite Element Solution (FES2012) hydrodynamic model. Combining these components, a set of extreme sea levels is derived, described by Gumbel distribution parameters based on annual maxima. The dataset is validated with tide gauges data. It shows a good agreement with a slight general underestimation of extreme levels, more profound at lower latitudes. This is caused by the fact that the meteorological data cannot resolve tropical cyclones. Thus the locations where the extreme water variability is dominated by such mechanisms cannot be described sufficiently by the model (Muis et al., 2016).

### 2.2.3 Wave Projections

To expand previous work, the effect of maximum wave height change towards the end of the century is implemented. To this aim, significant wave height projections data is used. Data consists of output from eight models (Table 2.1) and corresponds to three periods, 1980-2005 (historical), 2026-2045 (mid century) and 2080-2100 (end century). The wave model has a grid size of 1 degree and is forced

with 3-hour surface winds, and, linearly interpolated, monthly sea-ice concentration fields obtained from CMIP5. The models' output is 6-hourly projections of significant wave height, mean wave period and mean wave direction. First, annual maxima of significant wave height were obtained from the data for each period for the RCP 8.5 scenario. Data is available on the CSIRO website, in monthly NetCDF files containing all three parameters. Because of the amount of files and data, a MATLAB script was developed to download and process the projections. The script accesses the OPeNDAP server where the files are stored, downloads temporarily the significant wave heights for each month and computes the maximum monthly value. After doing this for all available months, it computes the annual maxima and stores them in a matrix, resulting in 20 annual maxima values per period per model. This process is repeated for all the models.

| | |
|---|---|
| ACCESS1.0 | Australian Community Climate and Earth System Simulator 1.0 |
| BCC-CSM1.1 | Beijing Climate Centre, Climate System Model, 1-1 |
| CNRM-CM5 | Centre National de Recherches Meteorologiques Coupled Global Climate Model, version 5 |
| GFDL-CM3 | Geophysical Fluid Dynamics Laboratory Coupled Physical Model |
| HadGEM2-ES | Hadley Centre Global Environmental Model 2, Earth System |
| INMCM4 | Institute of Numerical Mathematics Coupled Model, version 4.0 |
| MIROC5 | Model for Interdisciplinary Research on Climate, version 5 |
| MRI-CGCM3 | Meteorological Research Institute Coupled Atmosphere-Ocean General Circulation Model, version 3 |

**Table 2.1:** CMIP5 models used to obtain significant wave height projections for the RCP 8.5 scenario.

## 2.3 Methods

Comparison of GTSR and GESLA-2, as also the computation of allowances, were made at the nearest points between the involved datasets. The method of determining the nearest points between two datasets and computing the allowances for every case are presented below. In the case of including waves, an extra process of computing the wave maxima change distribution was needed.

### 2.3.1 Nearest points and Sea Level Change computation

The closest neighbor of each point of the tide gauges GESLA-2 dataset from the GTSR points is calculated using a MATLAB script. The script computes the distance of every GESLA-2 point with the whole GTSR grid and then it determines the GTSR point which corresponds to the minimum distance. Assuming a spherical earth, the distance $d_{mn}(i,j)$ of a point $P_{mn}$ to the point $P_{ij}$ at $(\lambda(i), \phi(j))$ is (Reerink et al., 2010):

$$d_{mn}(i,j) = R \ \arccos\left[\cos(\phi_{P_{mn}})\ cos(\phi_{P_{ij}})\ \cos(\lambda_{P_{mn}} - \lambda_{P_{ij}}) + \sin(\phi_{P_{mn}})\ \sin(\phi_{P_{ij}})\right] \quad (2.6)$$

where $\phi$ and $\lambda$ are expressed in radians. Finally, only the pairs of points with distances less than 100 km are kept for the comparison, yielding 636 pairs.

In order to compute a set of allowances using the reanalysis data, the process was repeated for the regional sea level change grid and the GTSR dataset, with a limit of 150 km. The reason for selecting a larger limit distance is that Sea Level Change grid is relatively smooth and thus this distance should retain the points between the two grids that are indeed well connected. Using this distance limit, 8869 GTSR points remain out of 9843 points initially, assigned to 2310 regional sea level change points. To reproduce the results of Slangen et al. (2017), the same process for Sea Level Change grid and GESLA-2, without a distance limit, leads to 652 nearest points.

Finally, to include the contribution of wave height maxima to the allowances, the process of computing the nearest points was repeated, again with a limit of 150 km, between GTSR, Sea Level Change grid and the wave projections grid. The output was 8305 points where wave-effect can be added to the allowance of the GTSR dataset, assigned to 2103 regional Sea Level Change points. It has to be noted that GTSR output does not include a wave contribution, hence there is no double counting of it.

After computing the nearest points for each case, Sea Level Change PDF including ice dynamics can be calculated. This is done by combining the regional Sea Level Change distributions with the ice dynamics of GIS, EAIS and WAIS. Since the contributing distributions are normal, as we use the IPCC values, the outcome is also an almost normal distribution. This distribution is finally used in computing the allowances.

### 2.3.2 Allowances using GTSR and GESLA-2 computation

As mentioned in section 2.1.1, we chose Gumbel distribution to describe extreme waters for the computation of allowances. A ongoing debate on this topic suggests that other distributions, like the Generalised Extreme Value distribution or the Pareto distribution are better in describing extremes, as the extra shape parameter leads to a more accurate fit (Wahl et al., 2017; Buchanan et al., 2016). Hunter et al. (2013) and Slangen et al. (2017) on the other hand support that most locations show a good Gumbel behavior. Moreover, Muis et al. (2016) compared Gumbel fit of GTSR data against measurements at selected locations with satisfactory results in most cases. For this project, following the framework of Slangen et al. (2017) we use a Gumbel distribution for describing extreme waters statistics.

Using the probability density function of the Gumbel distribution, eq. 2.3 with $\xi = 0$ representing the probability of no exceedances over z during a time period in equation 2.1, we get $N = \exp(\frac{\mu - z}{\lambda})$. If we then consider the sea level change up to some time (t) as $\Delta z + z'$ where $z'$ is the uncertainty described by a probability $P(z')$, we end up with a number of exceedances for the future of

$$N_{ov} = N \exp((\Delta z + \lambda ln(\int_{-\infty}^{\infty} P(z') \exp(\frac{z'}{\lambda}) dz'))/\lambda) \tag{2.7}$$

where the term

$$a = \lambda ln(\int_{-\infty}^{\infty} P(z') \exp(\frac{z'}{\lambda}) dz')) \tag{2.8}$$

represents the allowance needed to maintain the same number of exceedances over time [7]. Slangen et al. (2017), considering $z'$ as the total relative sea level change, applied the form of equation 2.8 for the cases of a normal distribution:

$$a = \mu_{SLC} + \frac{\sigma_{SLC}^2}{2\lambda} \tag{2.9}$$

and for a skewed distribution, described by a group of normal distributions with weights $w_i$:

$$a = \lambda ln(\sum_{i=1}^{n} w_i \exp(\frac{\mu_{SLC}}{\lambda} + \frac{\sigma_{SLC}^2}{2\lambda^2})) \tag{2.10}$$

### 2.3.3 Allowances using GTSR and wave maxima computation

In the case of including waves, an extra process of computing the wave maxima change distribution was needed. Then, the previous computation of allowances is altered accordingly.

#### Wave maxima change distribution computation

As mentioned in 2.2.3, significant wave height annual maxima were obtained for 8 CMIP5 models for historical and end century periods. Initially, a Gumbel fit was made for each model in order to investigate whether there are major discrepancies between them. Since all models yield the same patterns (Appendix C), the ensemble mean was computed for the two periods. Then, Gumbel fits were applied for each period, ending with two sets of Gumbel distributions. In order to determine a distribution that describes the change in significant wave height maxima between the two periods, statistical properties of mean and variance were used. More specifically, assuming two independent variables, the mean and variance of their subtraction is the subtraction of their means and variances respectively. First, mean and variance were computed at each point for both periods using equations 2.4 and 2.5. Then, the change distribution mean and variance were determined as:

$$\bar{x}_{change} = \bar{x}_{end} - \bar{x}_{hist} \tag{2.11}$$

$$\sigma_{change} = \sigma_{end} - \sigma_{hist} \tag{2.12}$$

Finally, using 2.4 and 2.5 again, mean and variance were converted to Gumbel location and scale parameters.

It has to be noted that the computation of distributions subtraction is feasible only in the case of the end century distribution having a larger variance than the historical one, so the resulting variance is positive. In the opposite case, variance of the distributions subtraction is negative, something that is invalid. The change distribution was computed for the part of the grid where the computed variance is positive, hence when the end century variance is larger than the historical. For the rest of the grid, Gumbel parameters of change distribution were assumed to be zero.

#### Allowances computation

To include the effect of wave maxima, the mean change cannot be ignored as in the case of tide and storm surges. Moreover, the variability of change probability works similarly to the uncertainty of the mean sea level change, as a large variability in wave maxima change demands a higher allowance to maintain the flooding risk. Thus, the mean and variance of the wave maxima change distribution were calculated according to equations 2.4 and 2.5. Using properties 2.11 and 2.12, the means and variances of regional sea level change and wave maxima change are combined at each point. GTSR scale parameter was used again to describe extreme waters. The process is summed up by the formula:

$$a_{GTSR-waves} = (z_{SLC} + z_{wave}) + \frac{\sigma_{SLC}^2 + \sigma_{wave}^2}{2\lambda} \tag{2.13}$$

The respective contributions by mean wave maxima change and its variability can be computed using the derivative of the allowance with respect to the wave maxima mean change and standard deviation:

$$\Delta a = \frac{\partial a}{\partial z_{wave}} \Delta z_{wave} + \frac{\partial a}{\partial \sigma_{wave}} \Delta \sigma_{wave} \tag{2.14}$$

where $\Delta z_{wave} = z_{wave}$ and $\Delta \sigma_{wave} = \sigma_{wave}$. From equation 2.13 we find $\frac{\partial a}{\partial z_{wave}} = 1$ and $\frac{\partial a}{\partial \sigma_{wave}} = \frac{\sigma_{wave}}{\lambda}$, hence we get:

$$\Delta a = \Delta z_{wave} + \frac{\sigma_{wave}}{\lambda} \Delta \sigma_{wave} \tag{2.15}$$

and the contributions of the wave maxima mean change and standard deviation are $\frac{\Delta z_{wave}}{\Delta a}$ and $\frac{\frac{\sigma_{wave}}{\lambda}\Delta\sigma_{wave}}{\Delta a}$.

### 2.3.4 Change in exceedance frequency

Having computed an allowance for a future year, for this project the year 2100, it can be used to calculate the change in frequency of exceeding a certain sea level at this time in case the allowance is not used. Using the allowance and the extreme waters variability, described here by the Gumbel scale parameter, at a certain gridpoint, the change in the frequency of extreme events can be computed as (Slangen et al., 2017):

$$N = \exp(\frac{a}{\lambda}) \tag{2.16}$$

This implies that if $N = 10^4$, an extreme event which now takes place once every 10000 years will occur once every year if the coastal infrastructure is not increased by the allowance.

Chapter 3

# GTSR and GESLA-2 datasets comparison

Data from GTSR and GESLA-2 were compared at their nearest points, setting a distance limit of 100 km. The respective Gumbel parameters and PDFs are compared at selected locations.

## 3.1 Comparison at specific locations

The next Figure (3.2) shows the PDFs of the two datasets, computed according to equation 2.3, for nine tide gauge locations (Figure 3.1) mentioned and investigated by Church et al. (2013) due to the long sea level records available. Additionally, Table 3.1 contains the values for the Gumbel location and scale parameter, $\mu$ and $\lambda$ respectively, at every location.

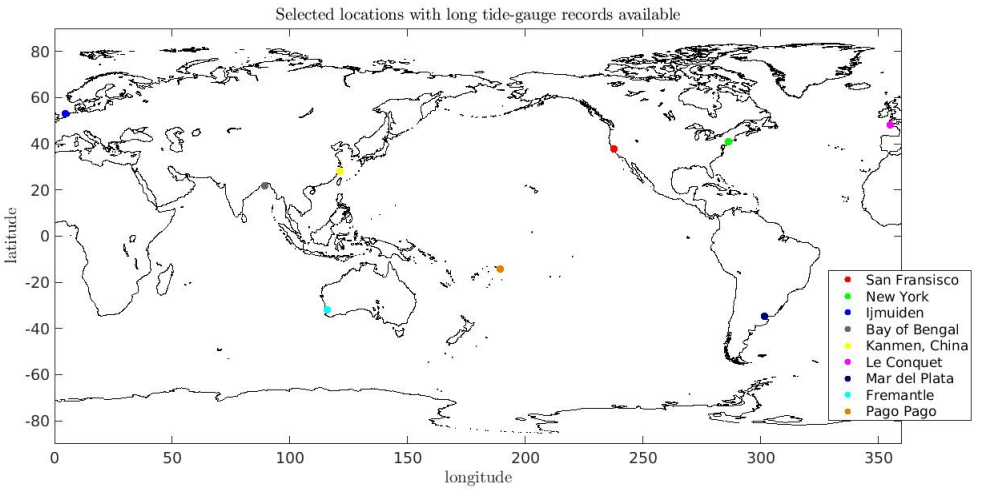


**Figure 3.1:** Nine tide gauge locations with long records available chosen to investigate.

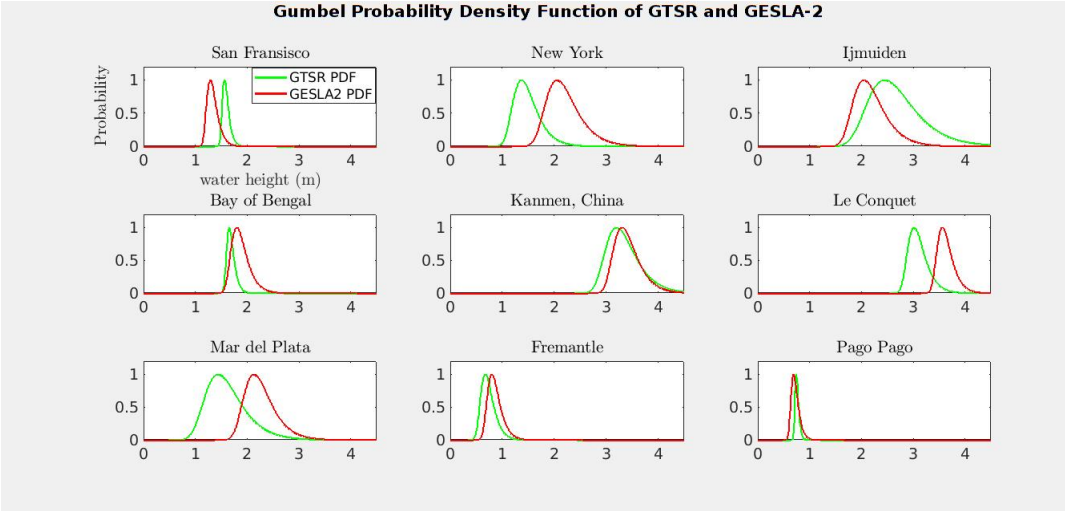


**Figure 3.2:** Gumbel Probability Density Functions of GTSR and GESLA-2 at nine selected tide gauge locations.

| | GESLA-2 $\mu$ | GTSR $\mu$ | GESLA-2 $\lambda$ | GTSR $\lambda$ |
|---|---|---|---|---|
| San Fransisco | 1.28 | 1.56 | 0.09 | 0.06 |
| New York | 2.05 | 1.36 | 0.28 | 0.21 |
| IJmuiden | 2.04 | 2.45 | 0.27 | 0.43 |
| Bay of Bengal | 1.79 | 1.65 | 0.14 | 0.07 |
| Kanmen, China | 3.3 | 3.19 | 0.21 | 0.27 |
| Le Conquet | 3.55 | 3.01 | 0.13 | 0.16 |
| Mar del Plata | 2.12 | 1.43 | 0.25 | 0.33 |
| Fremantle | 0.79 | 0.67 | 0.11 | 0.11 |
| Pago Pago | 0.68 | 0.73 | 0.06 | 0.03 |

**Table 3.1:** Gumbel location and scale parameter of GTSR and GESLA-2 distributions at the nine selected locations showed in Figure 3.1.

In terms of the distribution peak, best agreement is found at Bay of Bengal, Kanmen, Freemantle and Pago Pago, while for New York, Mar del Plata and Le Conquet GTSR underestimates the position of the peak by a bit less than 1 meter. There are also cases where GESLA-2 has a lower peak, more specifically at San Fransisco and IJmuiden, by about 0.3-0.5 m. Regarding the variability of the distribution, and consequently the Gumbel scale parameter, GTSR has a narrower distribution, hence a smaller scale parameter, at San Fransisco, Bay of Bengal and Pago Pago. These are locations both dominated by tropical cyclones, except for San Fransisco, and showing low variability, which are the main cases where GTSR underestimates variability of extreme waters (Muis et al., 2016). On the other hand, for Mar del Plata the GTSR shows a larger extremes variability, something confirmed also by the values in Table 3.1. For the rest of the locations variability appears to be almost similar for the two datasets. The relation between the two datasets parameters at a global extent will be discussed in the next section.

## 3.2 Gumbel parameters comparison on the global scale

First, it should be noted that GTSR covers most of the global coastline while GESLA-2 points are limited, thus in the largest part of the map there are no GESLA-2 values to compare with GTSR values. It is relatively clear from Figures 3.3, 3.4 and 3.5 that GESLA-2 scale parameter is larger at low latitudes, most likely because of the underestimation of the scale parameter at these latitudes by GTSR as tropical cyclones are not resolved, while at higher latitudes GTSR scale parameter appears to be larger in most locations. Also, we see a meridional pattern for both datasets with increasing values towards the poles, implying more variability in the water levels. In Figure 3.5, it can be seen that the difference of scale parameters from the two datasets varies in most cases between -0.08 and 0.08. Most of the negative values, and thus a larger GTSR scale parameter, are observed at Europe and North America's west coast. These two areas are characterized by a large tidal range and a high storm activity respectively, thus the variability of extreme levels because of these phenomena is well resolved by GTSR. Positive values are mostly located at the western Pacific Ocean and the central America area, locations where the extremes are dominated by tropical cyclones and thus GTSR yields a lower scale parameter than GESLA-2. Figure 3.6 shows that the most significant differences occur at the western Pacific and central America areas as the largest ratios of GESLA-2 over GTSR scale parameter are located there. In these areas, GESLA-2 scale can be up to 4 times larger, indicating the heavy underestimation by GTSR near the equator. For the rest of the global coastline, ratio varies mostly between 0.5 and 2.

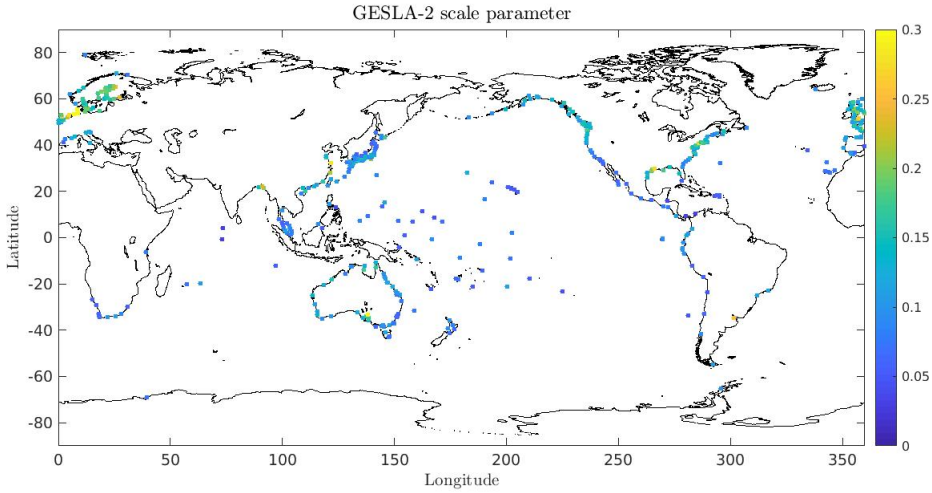


**Figure 3.3:** GESLA-2 data scale parameter at all points.

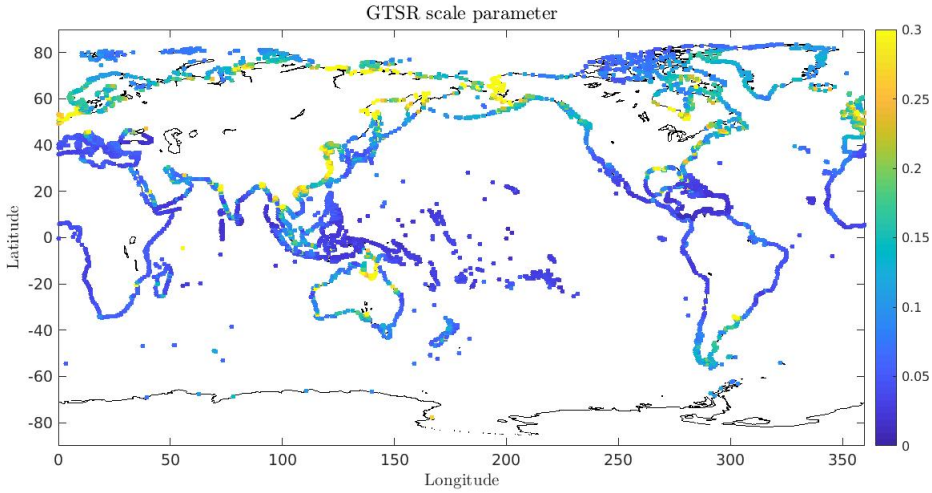


**Figure 3.4:** GTSR data scale parameter at all points.

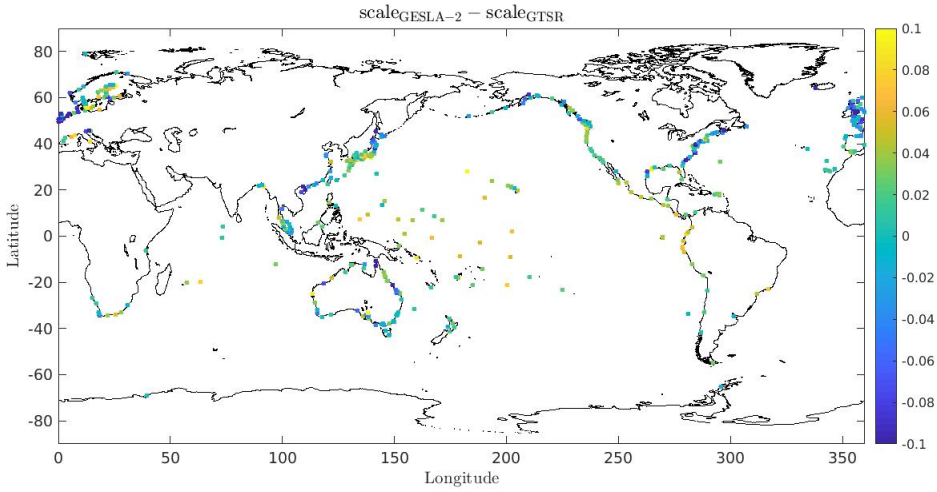


**Figure 3.5:** GESLA-2 and GTSR data scale parameter difference at all points.

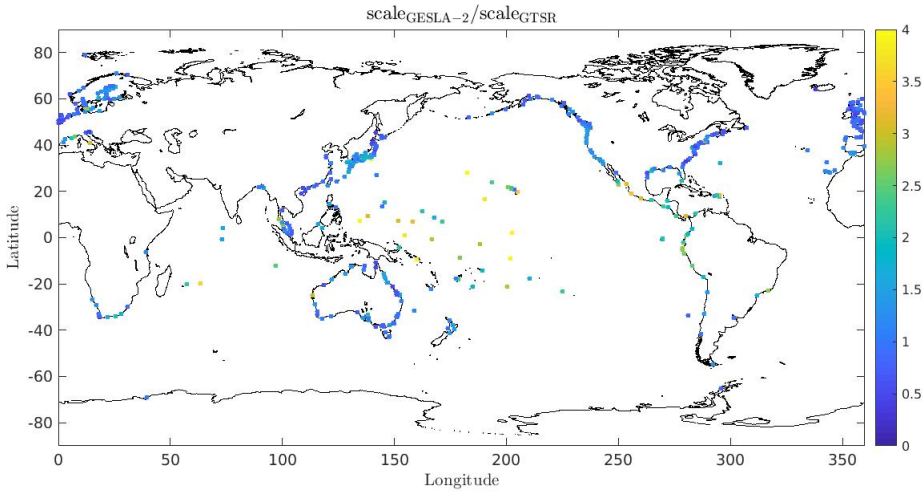


**Figure 3.6:** GESLA-2 and GTSR data scale parameter ratio at all points.

Figures 3.7 and 3.8 show the location parameters of GESLA-2 and GTSR at all points, while Figures 3.9 and 3.10 show GESLA-2 and GTSR location parameters difference and ratio at the computed overlapping points. We observe that there is no clear meridional pattern seen in neither of the two datasets. For GTSR, the lowest values, close to zero, are located mostly in the Mediterranean and the area of central America, indicating again the underestimation of extremes at tropical cyclone dominated areas. High values, more than 2.5, are found in several locations, such as North Australia, Northwest Europe, Argentina and the south coast of Alaska. These areas are known for a large tidal range (Matthews, 2013), something that is in agreement with the magnitude of the location parameter. For the majority of points the ratio of location parameters is between 0.8 and 1.2 and the absolute difference less than 0.2 m. In terms of difference, GESLA-2 location parameters seem to be larger than the GTSR ones at Northwestern Europe and at a specific location of Southeast Australia. However, the ratio map only shows a significant difference in terms of magnitude at the Australia points. The ratio map also reveals ratios higher than 1.4 at more dispersed locations like Argentina and the Baltic Sea. GTSR location parameters dominate only at specific points with no obvious pattern, as seen in both Figures 3.9 and 3.10.

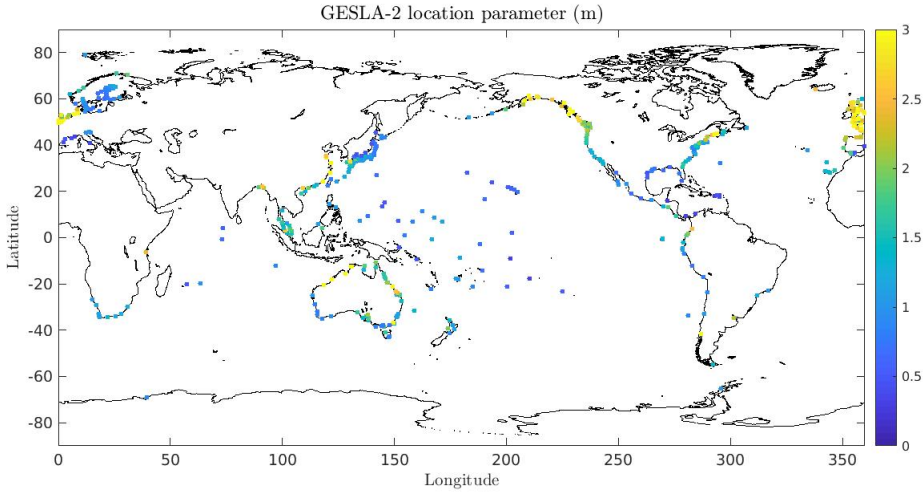


**Figure 3.7:** GESLA-2 data location parameter at all points.

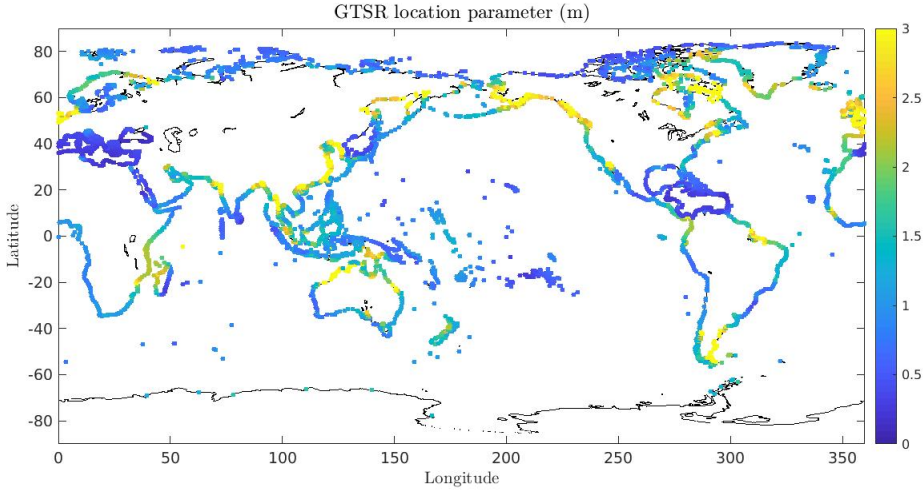


**Figure 3.8:** GTSR data location parameter at all points.

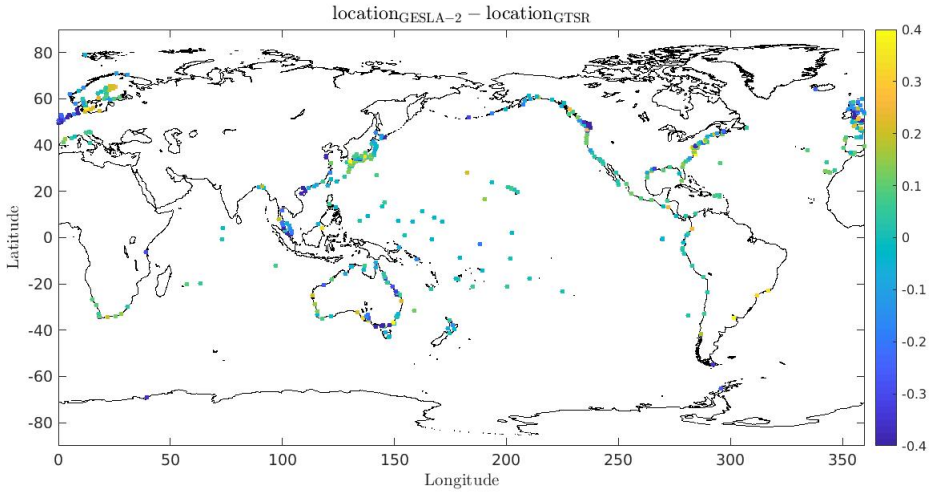


**Figure 3.9:** GESLA-2 and GTSR data location parameter difference at all points.

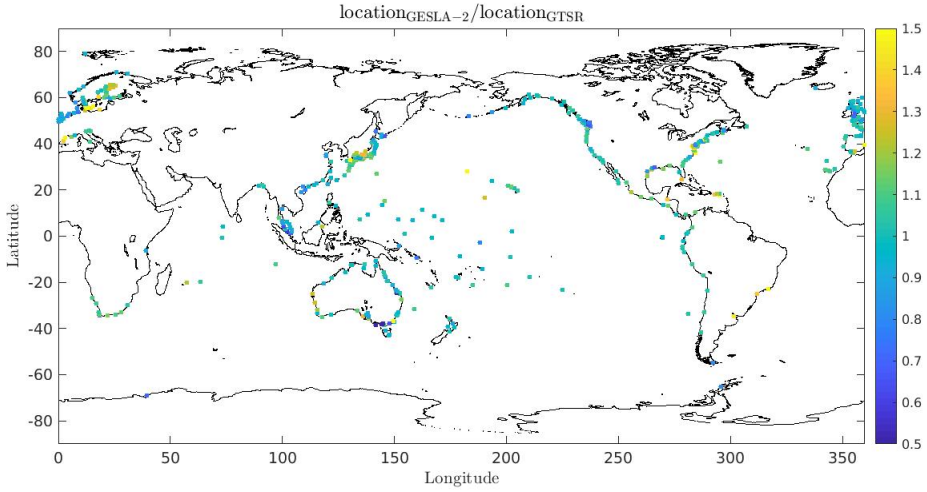


**Figure 3.10:** GESLA-2 and GTSR data location parameter ratio at all points.

Gumbel parameters of both datasets were also compared by plotting them against each other (Figures 3.11,3.13) as well as their ratio against latitude (Figures 3.12,3.14). Observing the scale parameters plot, there appears to be enough dispersion (Figure 3.11). Most of the points though seem to be in good agreement, considering also the magnitude of the axes. GTSR appears to underestimate the lower variability points, as seen in Figure 3.11 for a scale parameter lower than 0.1. This is also reported by Muis et al Muis et al. (2016), while for larger variance there is no clear relation between the two datasets. Moreover, the linear regression performed resulted in a slope of 0.883, which shows good relation of the two datasets scale parameters at many points. The group of underestimated variability points by GTSR though leads to a low $R^2$ value of 0.37, as these points are not represented by the linear fit. The relation between GTSR data and latitude mentioned previously can be observed in Figure 3.12 as a decrease of the ratio towards high latitudes, with values up to about 6.5 near the equator.

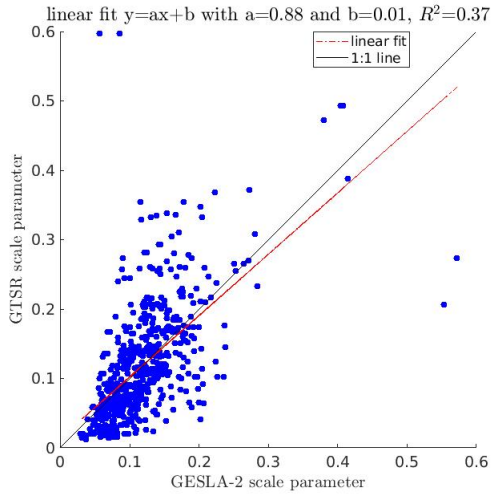


**Figure 3.11:** GESLA-2 scale parameter against GTSR scale parameter at the datasets' nearest points, with linear fit.

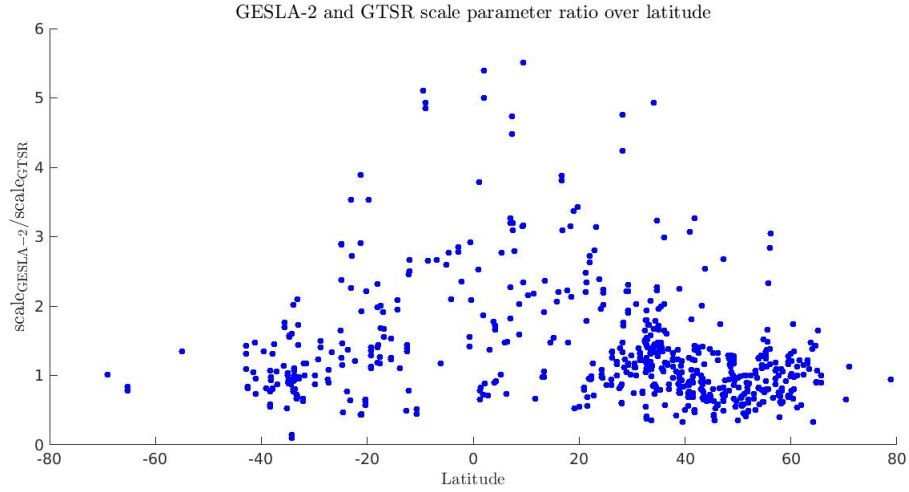


**Figure 3.12:** GESLA-2 and GTSR data scale parameter ratio at the datasets' nearest points against latitude.

Location parameters of Figure 3.13 show significantly less scatter than the scale parameters. Linear regression resulted in a slope of 1.016 which is also closer to the ideal value of 1 than the 0.883 computed for scale parameters. In this case, $R^2$ is 0.92, meaning that most of the points are described well by the linear fit. Also, there appears to be a small branch of points, almost parallel to the main group, with larger values for the GTSR location parameters by about 0.5-1 meter. As seen in the maps though, these points do not create some specific patterns. Moreover, unlike the relation between the scale parameters and latitude, no similar finding occurs from Figure 3.14. At most latitudes, ratios obtain values around 1. A slightly higher dispersion is observed at latitudes northern than 30 degrees, but at the same area there are more points available. It is clear from the above findings that the underestimation at tropical cyclone dominated areas by the GTSR is mostly in terms of variability than magnitude.

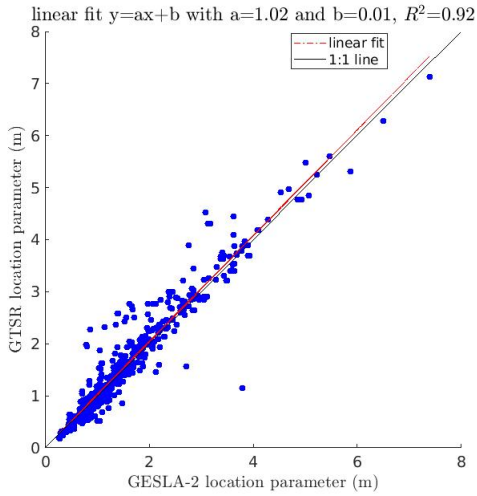


**Figure 3.13:** GESLA-2 location parameter against GTSR location parameter at the datasets' nearest points, with linear fit.

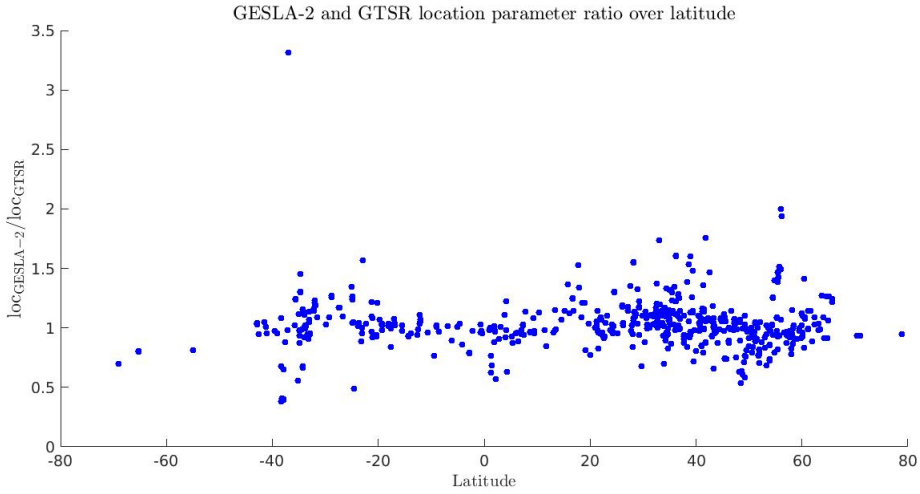


**Figure 3.14:** GESLA-2 and GTSR data scale parameter ratio at the datasets' nearest points against latitude.

Chapter 4

# GTSR and GESLA-2 allowances

After comparing GTSR and GESLA-2 datasets, we use GTSR to compute a set of allowances. This set is compared to the one using GESLA-2 data made by Slangen et al. (2017) and reproduced here. Additionally, a continental analysis is performed to the GTSR allowances. Finally, we investigate the percentage of points in our grid that will be affected by a strong increase in the exceedance frequency at the end of the century.

## 4.1 Results on the global scale

Figure 4.1 represents the allowances results using the GTSR and GESLA-2 datasets as extreme waters data. For the majority of coastline, allowances are between 1 and 1.5 meter. This appears to be the case for the largest parts of Europe, Asia, North America and Australia. Africa shows larger values, up to around 1.8 at its coastline between -10 and 10 degrees latitude. South America has also some similar high values at its northwestern and central eastern coasts. The areas with the highest allowances, up to more than 2 meters, are the Caribbean, North Greenland, Maldives and a large area starting from Indonesia and covering most part of the western and central Pacific Ocean. For all the aforementioned areas, low values of GTSR scale parameter are observed in Figure 3.4, though for North Greenland an important factor also appears to be the high uncertainty of regional SLC in this area(Slangen et al., 2014). Moreover, some areas with a high tidal range (Matthews, 2013), like the coast of Mozambique in Africa, the Gulf of Alaska and the southern end of South America, are observed to have lower allowances than their surroundings, a finding consisting with a high variability in extreme water levels. Also, these areas are easier to point out due to the fact that they are far from the equator and the local extreme levels behavior is not affected by the GTSR tropical cyclone underestimation.

Because of the limited amount of GESLA-2 points, we cannot deduct solid comparison conclusions for a large part of the map. We see though that along the coasts results are in satisfactory agreement in most of the places where we have points from both sets. The coastal areas that seem to show deviations between GESLA-2 and GTSR are the Caribbean, where we observe larger values for GTSR even more than 1 m, and the west coasts of southern North America and the northern South America where GTSR allowances appear again larger, with differences around 1 m. The high allowances areas observed in the GTSR results at the east and west coasts of central Africa cannot be compared to GESLA-2 as there is no available data there. The most striking deviations occur far from the coasts, especially in the western Pacific Ocean. Reminding that the allowance for a normal

distribution of sea level rise projections is

$$a = z + \frac{\sigma^2}{2\lambda} \tag{4.1}$$

, the reason of these deviations appear to be twofold. First, as seen previously (Figures 3.3, 3.4), the western Pacific, as also the area around Indonesia is characterized by very low values of the scale parameter, less than 0.1 in most points for both datasets. A very low scale parameter can cause the second term of equation 4.1 to blow up. Moreover, Figure 3.6 shows important differences between GTSR and GESLA-2, with the first one having smaller values. These two facts, combined with the presence of $\lambda$ in the upper equation in the denominator, cause the large differences seen in terms of allowances.

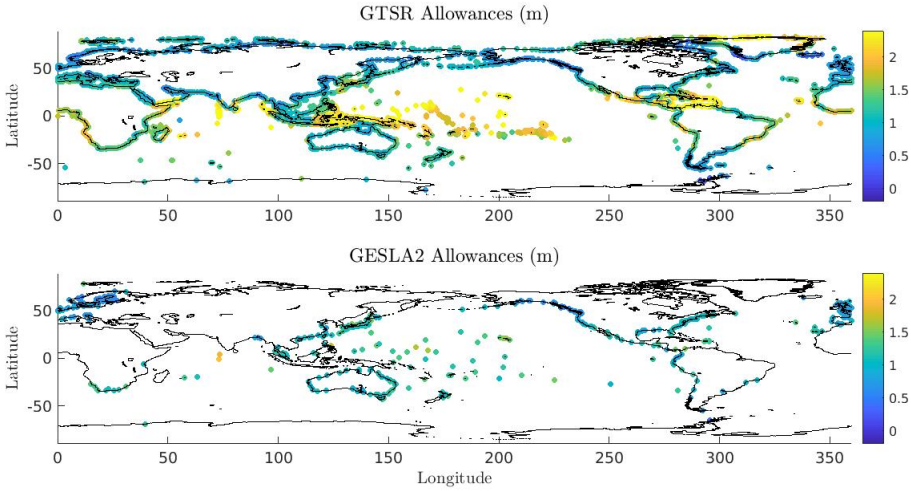


**Figure 4.1:** Upper: Global allowances computed using sea level change projections and GTSR data. Lower: Global allowances computed using sea level change projections and GESLA data.

Focusing on Europe (Figure 4.2), we see two different groups of results. Northern Europe is mostly characterized by allowances between 0.6 and 0.8 meters, values that reach south to Gibraltar. Mediterranean shows larger values, between 1 and more than 1.2 meters, except the cases of the north Adriatic sea and the coast around the Greek-Turkish borders where the allowances are around 0.8 meters.

There seems to be a good agreement between the two datasets particularly for the north coasts. In the Mediterranean, the limited amount of GESLA-2 data makes the comparison uncertain. Most of the sparse available points in the area have close values to the GTSR ones, though in areas with dense high GTSR allowances not enough GESLA-2 points exist to compare and make a robust conclusion at what extent this is connected to the GTSR scale parameter underestimation. It is important to mention though that Mediterranean shows low extremes variability, thus it may be that GTSR underestimates the scale parameter which results in a higher allowance.

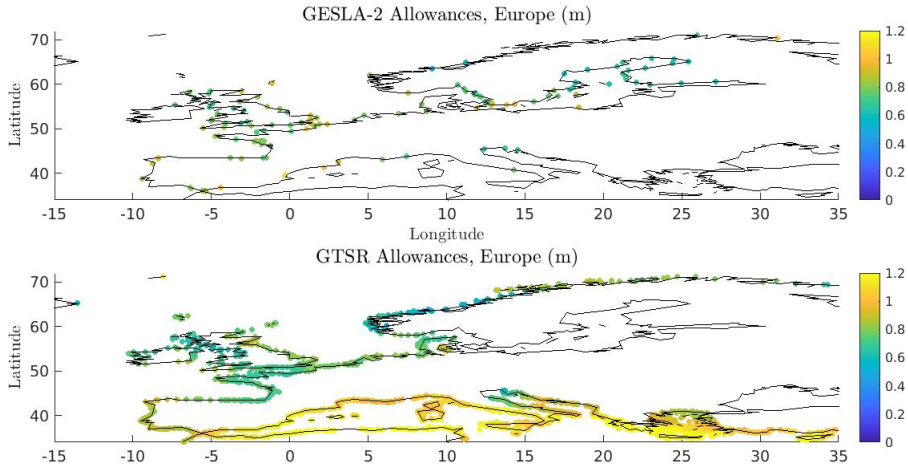


**Figure 4.2:** Upper: Allowances computed using sea level change projections and GTSR data in Europe area. Lower: Allowances computed using sea level change projections and GESLA data in Europe area.

## 4.2 Continental Analysis

Areas representing Europe, Asia, Africa, North and South America, Oceania and Antarctica were selected as shown in Figure 4.3. Allowances of each continental area were plotted against latitude to investigate a possible correlation. Linear trends are computed, with a unit of allowance meter per degree latitude.

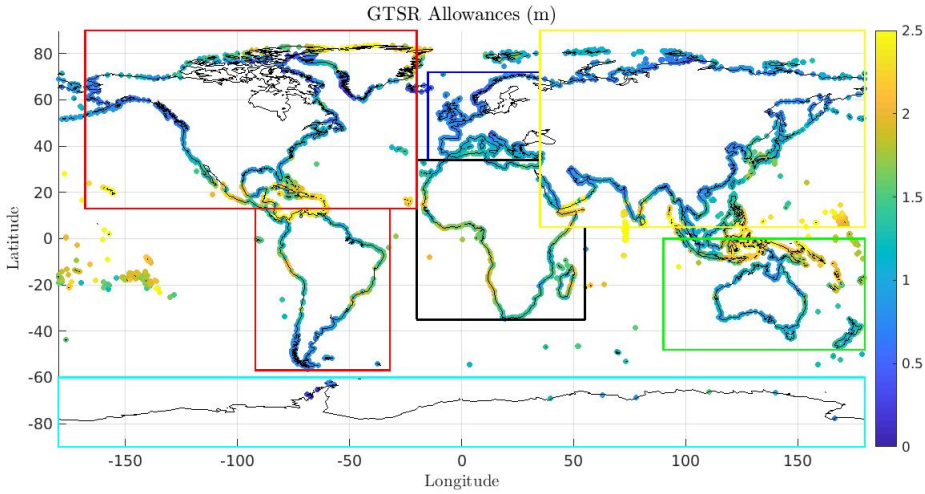


**Figure 4.3:** Allowances computed using sea level change projections and GTSR data with selection of continents.

As seen in Figures 4.4-4.9, there is an increasing trend towards the equator for every continent. Antarctica was not investigated as there are very few points at this area. Trends are separated for North and South Hemisphere in every continent. Slopes take values of about 0.01 to 0.02 meters per

degrees latitude in all cases except North America where it is 0.009 and the Southern Hemisphere part of Africa with about 0.002. For North America, this is caused by the high allowances area of north Greenland (Figure 4.1). Moreover, it is interesting to point out that for a few points of the northern part of North America, around 60 degrees, allowances take negative values. This happens because of the land uplift at this area(Hunter et al., 2013). For Africa, low allowances computed at the coast of Tanzania lead to the small trend for the South Hemisphere. Another anomaly is observed in Figure 4.8, where the area of Caribbean with the high allowances mentioned before is visible above 10 degrees of latitude. Thus, in this case the trend for the North Hemisphere part was not computed. The highest trends are observed in Europe and Oceania (0.018). For Europe this is another visualization of the difference between the northern and southern part mentioned in the previous section. For Oceania, which as seen in Figure 4.3 captures also a part of Singapore and Indonesia, the high allowances at these areas as also at the islands of West Pacific Ocean are the cause of the high trend.

The consistency of these increasing trends within the range mentioned is a more important finding than their sole existence which could be due to the underestimation of variability by the GTSR near the equator. Neither regional SLC projections nor their uncertainty show a similar pattern on map (Slangen et al., 2014). It would be interesting for these trends to be further investigated using future allowance sets in order to confirm their occurrence and exact source.

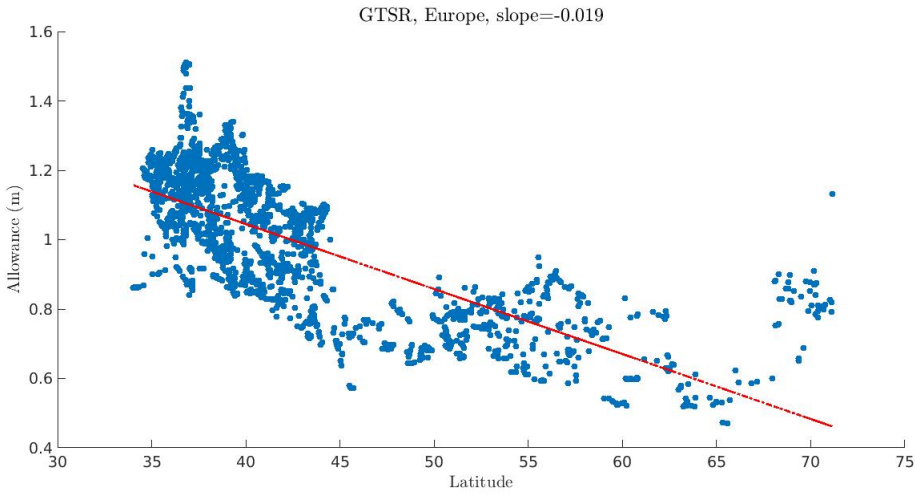


**Figure 4.4:** Allowances computed using sea level change projections and GTSR data versus latitude, Europe.

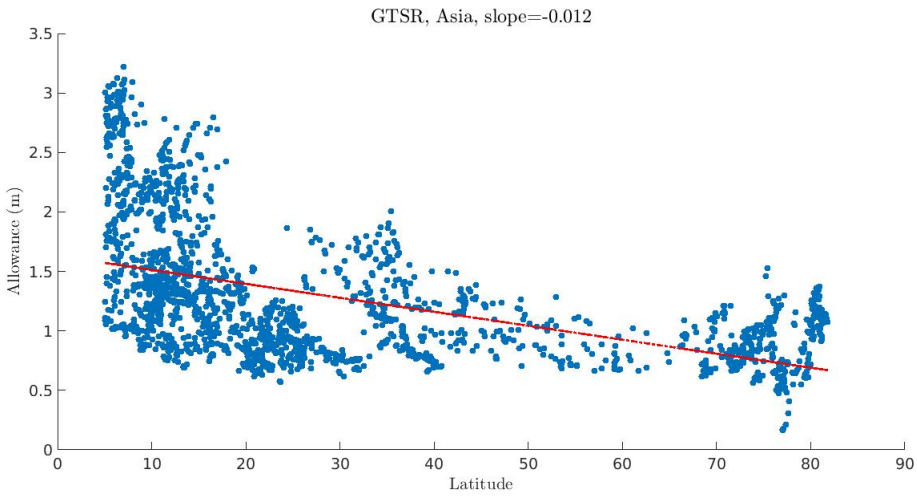


**Figure 4.5:** Allowances computed using sea level change projections and GTSR data versus latitude, Asia.

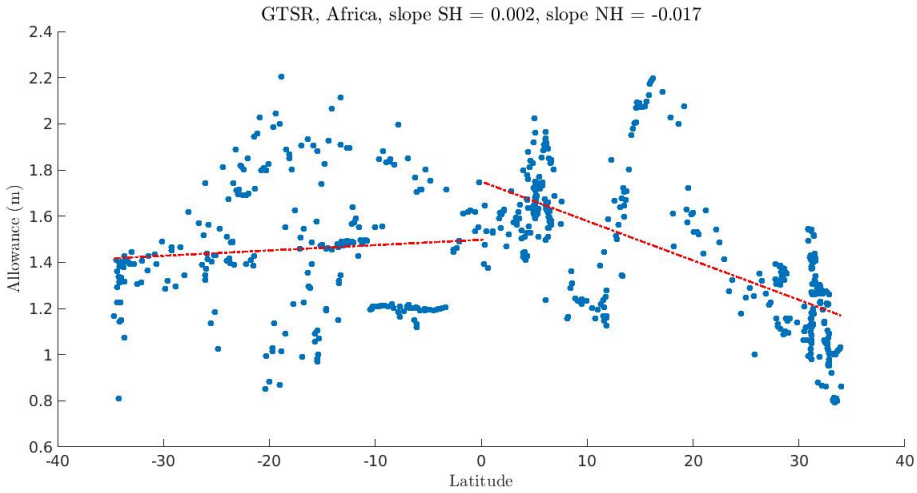


**Figure 4.6:** Allowances computed using sea level change projections and GTSR data versus latitude, Africa.

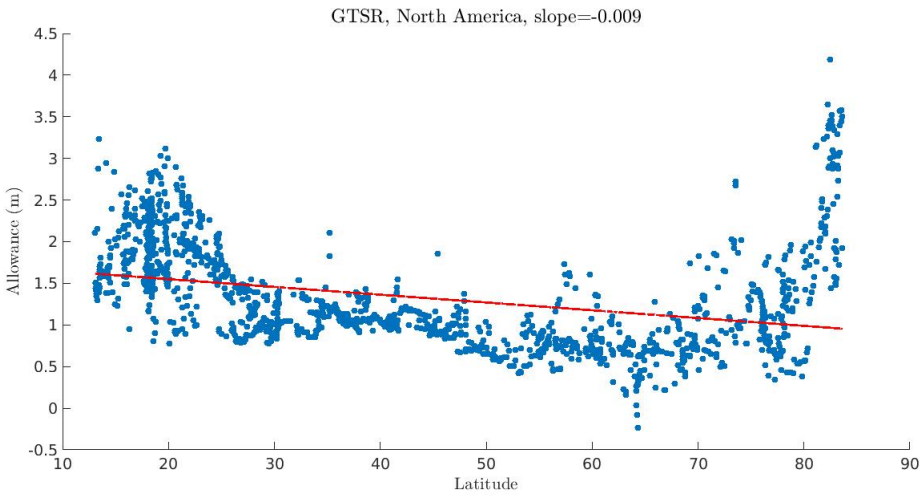


**Figure 4.7:** Allowances computed using sea level change projections and GTSR data versus latitude, North America.

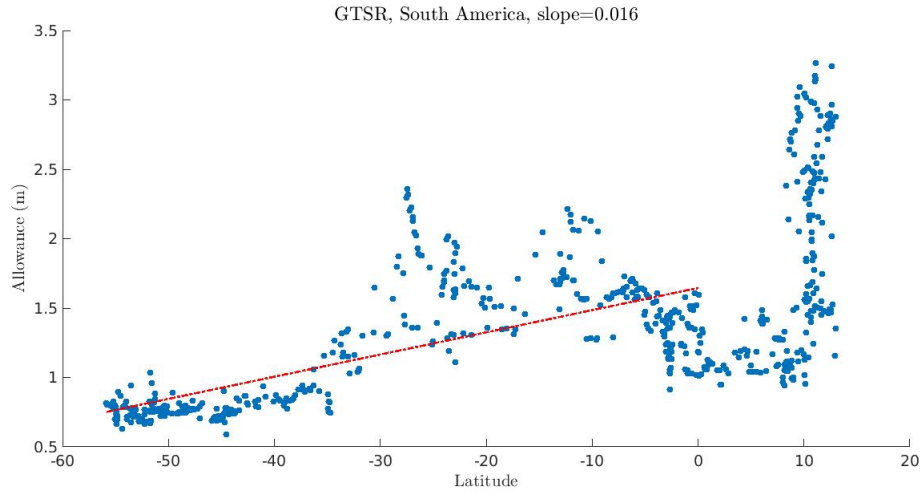


**Figure 4.8:** Allowances computed using sea level change projections and GTSR data versus latitude, South America.

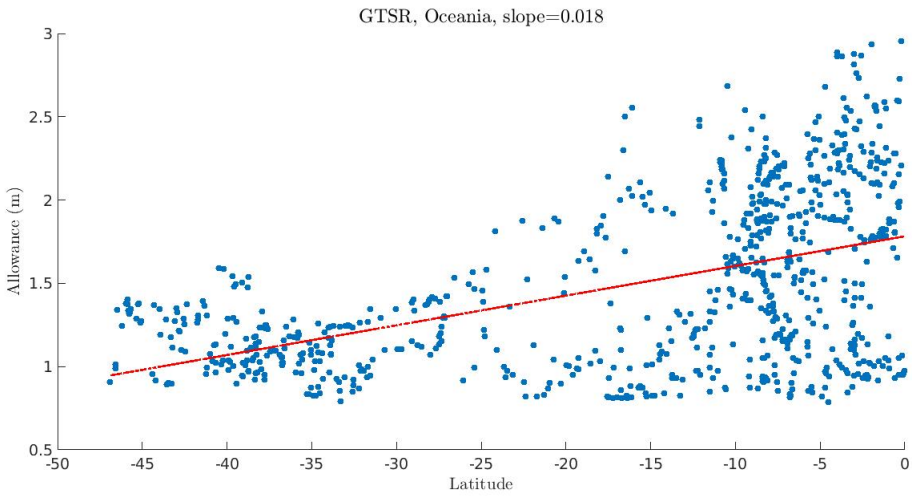


**Figure 4.9:** Allowances computed using sea level change projections and GTSR data versus latitude, Oceania.

## 4.3 Change in extreme events frequency

Using equation 2.16 and the computed set of allowances for GTSR, we can calculate the percentage of points that will surpass a certain change in frequency of extreme events. The chosen changes are $10^3$ and $10^4$, similarly to Slangen et al. (2017). That means for the calculated percentages, events occurring once per 1000 and 10000 years respectively, at the end of the century will occur once per year without the use of allowances. The results are 78.1% for $N = 10^3$ and 71.5% of the points for $N = 10^4$. The respective results using GESLA-2 were 67% and 50%, thus extending the grid using GTSR the percentages are significantly larger.

Chapter 5

# GTSR including significant wave height maxima change allowances

The next step is to include the wave maxima change between the present and the end of the century. The Gumbel distribution describing this change as well as the respective set of allowances are presented. A continental analysis is also performed to this set to investigate changes comparing to the previous case, without wave change. Similarly, results for percentage of points with a large exceedance frequency change are compared. Finally, we focus on nine specific locations where we investigate all sets of allowances along with the SLC distribution.

## 5.1 Significant Wave Height maxima change distribution results

Figures 5.1, 5.2 show the results for the distribution describing the change in wave height maxima between the historical period and the end of the century, computed as described in subsection 2.3.3. The distribution is expressed in terms of the Gumbel location and scale parameter. In order to distinguish the positive and negative values of the location parameter, a special colormap was created, assigning green color to positive values and red to negative ones. A positive value indicates an increase in the peak of wave maxima distribution towards the end of the century, while a negative value means a decrease.

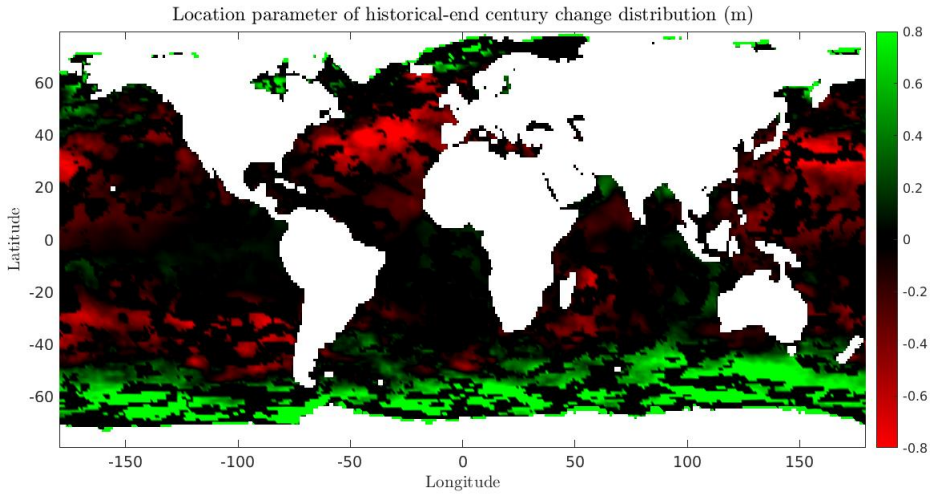


**Figure 5.1:** Location parameter of the Gumbel distribution describing the change in significant wave height maxima from historical to end century period. Positive values indicate an increase over time.

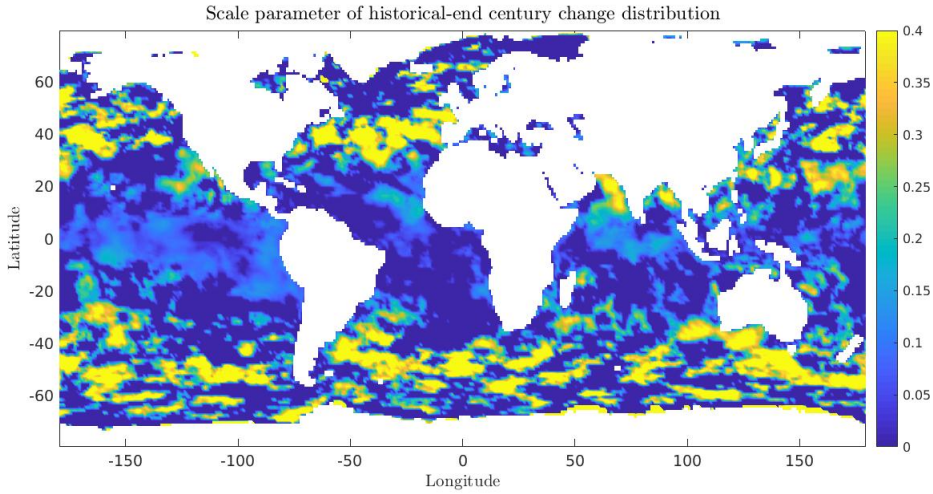


**Figure 5.2:** Scale parameter of the Gumbel distribution describing the change in significant wave height maxima from historical to end century period.

In terms of the location parameter, thus the peak of the change distribution, there are two main belts of increase, as also two of decrease. The first ones are located at high latitudes, $> 50°N$ or $< 50°S$. The two zones of decrease are found at lower latitudes, one between 0 and about 45 degrees, and the other between -20 and -50 degrees latitude. It can be observed that on average the increase areas are stronger than the decrease ones reaching in most points values of 0.8 to more than 1 meter, while the decrease remains mostly between -0.4 and -0.8 meters.

In terms of the scale parameter, the lower values, less than 0.2, are located mostly at the tropics. At higher latitudes, most points have a scale parameter around 0.4, meaning a higher variability in wave height maxima change probability. It is clear from Figures 5.1 and 5.2 that there are three areas of relatively clear behavior. For latitudes between about 30 and 50 degrees, a relatively large decrease

in the peak of maxima is observed, accompanied by a large variability in the change between historical period and end of century. A second characteristic area is the zone around -60 degrees latitude, where the peak of maxima distribution is increasing up to more than 1 meter, while there is also high variability. The same behavior is found in the northern Indian Ocean, more specifically the Bay of Bengal and the north part of the Arabic Sea. Results show similarities with the patterns of changes in annual maximum significant wave height computed by Wang et al. (2014). Small differences are caused by the facts that Wang et al used the ensemble of a larger number of models, as also computed the change as a percentage and not as a probability distribution as done in this project. Also, our computed patterns show similarities with the change in surface wind speed between the periods 2080–2100 and 1980–2005 under the RCP 8.5 scenario computed by Karnauskas et al. (2017). This indicates that the change in wave height maxima is driven mainly by the change in surface winds. After analyzing the results of the wave maxima change distribution, the new set of allowances taking this change in account follows.

## 5.2 GTSR and wave maxima change Allowances

### 5.2.1 Results on the global scale

Figure 5.3 shows the allowances computed using regional sea level change and GTSR along with the allowances including the change in wave height maxima between the historical period and the end of century.

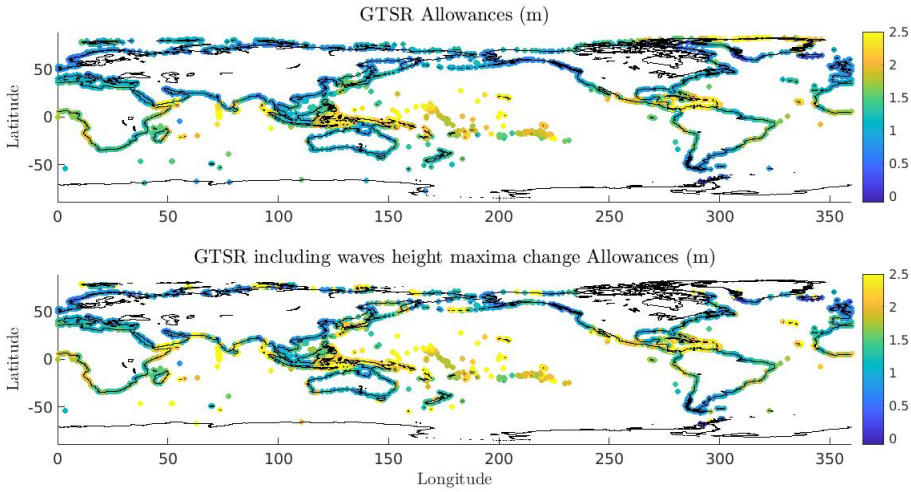


**Figure 5.3:** Upper: Allowances computed using sea level change projections and GTSR data. Lower: Allowances computed using sea level change projections, wave maxima change and GTSR data.

No many differences are observed between the two sets of allowances. This means for most areas the computation of the allowance is dominated by either regional sea level change or the extreme waters variability, and not by the change in wave maxima. Some areas where wave maxima change is important though can be seen. Several islands located around -50 degrees latitude are affected by an increase of their allowance of about 1 meter, thus flooding risk in these areas is heavily affected by the wave extremes change towards the end of the century caused by an in increase in wave height maxima. Another area of strong increase is found at the Bering Sea, the sea connecting Alaska with Russia, where for several of Andreanof Islands including wave maxima causes an increase of even

more than 1 meter in the allowances. Finally, points with similar high increase are found in the two parts of Indian Ocean mentioned in subsection 5.1, the north Arabic Sea and the Bay of Bengal. In all aforementioned areas, a strong increase in the mode of the wave maxima change distribution is observed. This is not the case for the Azores, which despite being within an area with a slight decrease in the location parameter of the change distribution, show an increased allowance. The reason for this is the high variability of the wave maxima change distribution in this area, with the scale parameter taking values higher than 0.4. This corresponds to a large variance in equation 2.13, thus increasing the allowance.

Focusing in Europe, in order to distinguish the points affected by wave maxima change, the difference between the two sets of allowances at their common points is plotted (Figure 5.4), as well as the contribution by mean wave maxima change and its standard deviation (Figures 5.5,5.6).

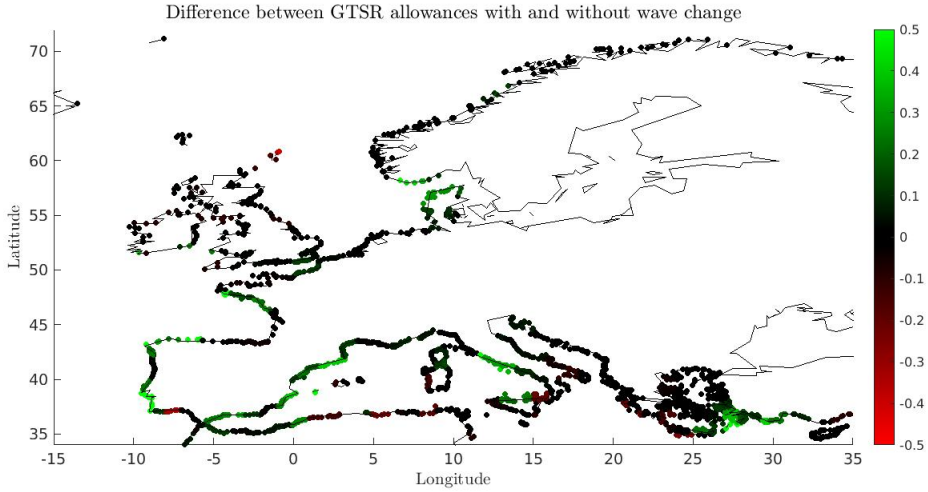


**Figure 5.4:** Differences between allowances using sea level change projections and GTSR data, with and without including wave height maxima change, Europe.

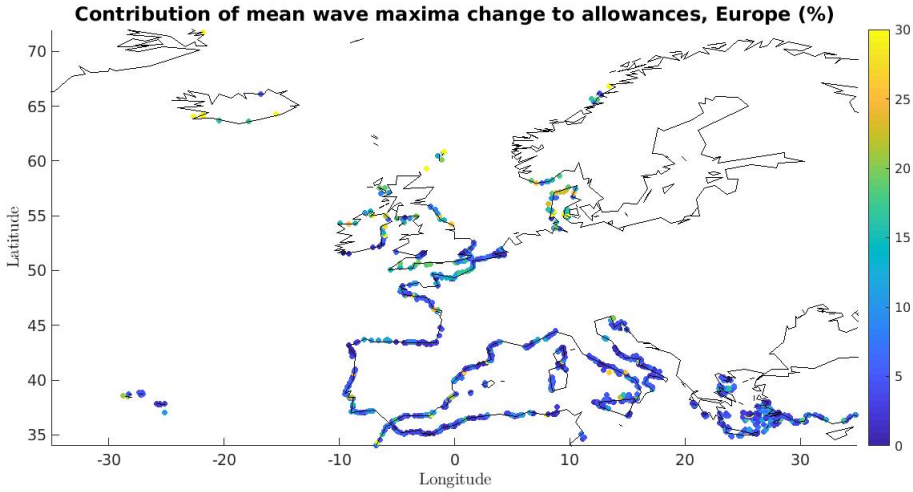


**Figure 5.5:** Percentage of the additional allowance $\Delta a$ due to the wave maxima change contributed by the mean change for Europe.

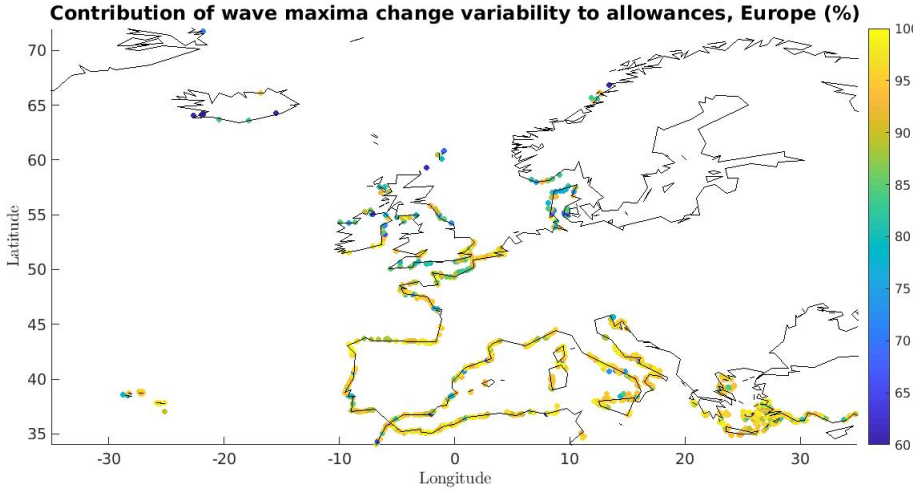


**Figure 5.6:** Percentage of the additional allowance $\Delta a$ due to the wave maxima change contributed by the standard deviation of the change distribution for Europe.

Both increasing and decreasing allowance points are observed in Figure 5.4 after including waves change in computation. Most areas of increase are located in South Europe. Southeast Aegean Sea, the west coast of Central Italy and the most part of Spain and Portugal coastline show an increase of about 0.3-0.6 meters. For North Europe, the two main areas of increase are the coast of Denmark with a difference of about 0.3 m, as also the south edge of Norway with a higher increase of about 0.5 m. In terms of decreasing allowances due to wave extremes change towards the end of century, most cases are observed within the Mediterranean, at the North Africa part but also at North Sicily and the west coast of Sardinia in Italy. These areas show a decrease by about 0.2 m, while there are two areas of larger decrease, one just west of Gibraltar and the Shetland Islands at the northernmost part of the UK, where including the change in wave extremes allowances decrease by about 0.3 to

0.4 meters.

Interestingly, from Figure 5.1 it can be seen that the location parameter, thus the peak of the wave extremes change distribution, is negative for the whole part of Europe where it was computed. This leads to the conclusion that the high variability of the change distribution compensates for the negative change in location parameter, resulting in a higher allowance in order to cover the existing probability of an increase in wave height maxima. The conclusion is confirmed by Figures 5.5 and 5.6. It can be observed that for most part of Europe, the effect of wave maxima change in the allowances is mostly due to the variability of the change, represented by the standard deviation, and not the mean change. Another example for this are the Azores which are located in a negative location parameter area (Figure 5.1) and despite that show an increase in the allowance (Figure 5.3). The important influence of wave maxima change variability to allowances makes the need for a better accuracy in the extreme waters variability. This is due to the fact that the extreme waters variability is in the denominator of equation 2.13, and hence a possibly underestimated value can magnify the effect of wave change standard deviation. The next step is to check whether a relation between the new set of allowances and latitude exists.

### 5.2.2 Continental Analysis

As seen in the previous subsection, wave height maxima change from the historical period to the end of century affects mostly areas in Southern Europe with an increase in most locations and a, lower in average, decrease in some others. This can be observed also in Figure 5.8, where we see the points with a high additional allowance of up to about 3 meters due to waves change for lower latitudes. No robust pattern of the additional allowance with latitude is visible though. This is also captured in the latitudinal plot of allowances (Figure 5.7). The higher dispersion observed due to the effect of including waves in some of the points leads to a small increase in the trend towards the equator of about 0.001 meters per degree latitude.

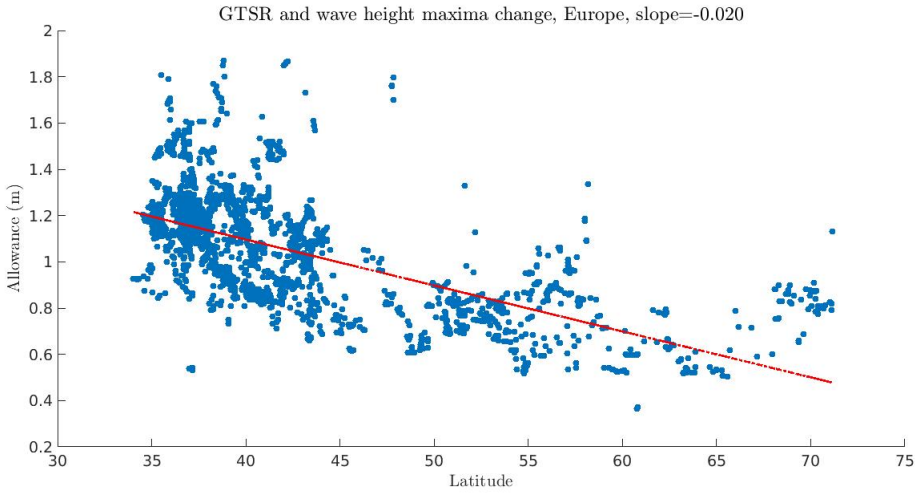


**Figure 5.7:** Allowances computed using sea level change projections, wave maxima change and GTSR data versus latitude, Europe.

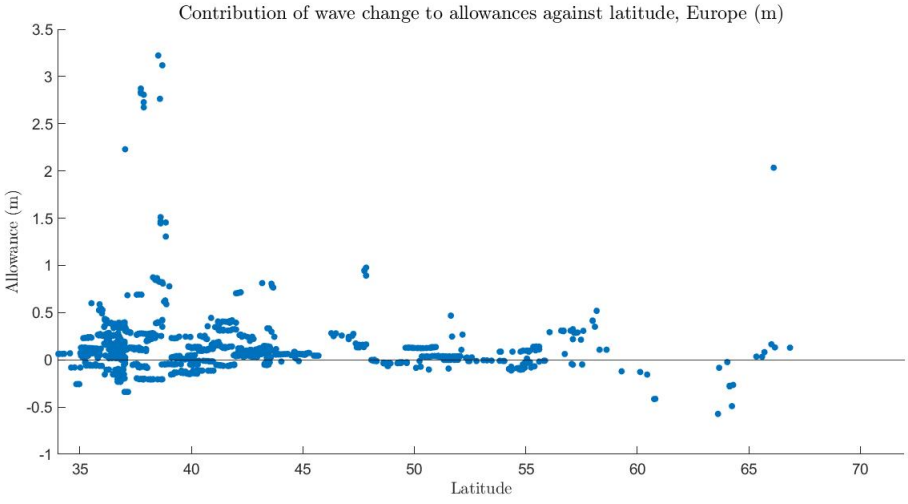


**Figure 5.8:** The additional allowance $\Delta a$ due to wave maxima change as calculated by equation 2.15 for Europe against latitude.

For the rest of the continents, small differences are observed in terms of equatorward trends. South America (Figure 5.9) and Oceania (Figure 5.10) show an increase and decrease of 0.001 respectively. For Oceania, this is most likely because of some points at the south coast affected by the high variability in the change of wave maxima giving higher allowances.

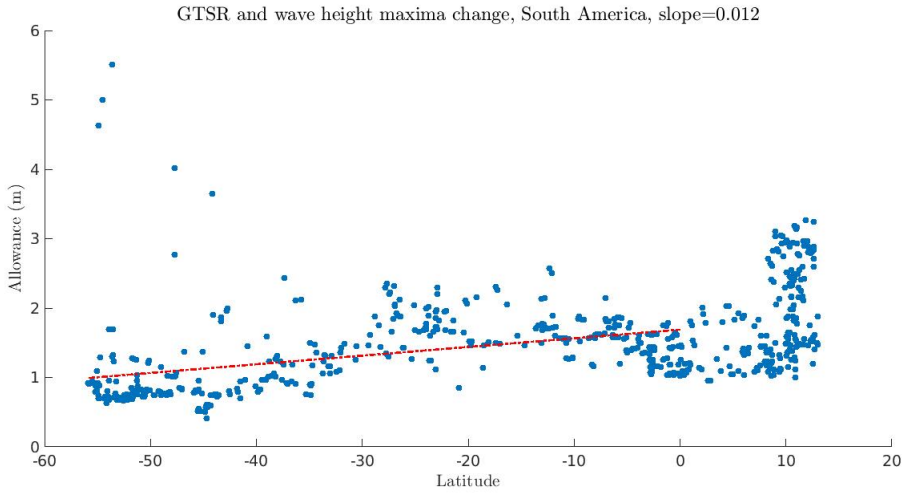


**Figure 5.9:** Allowances computed using sea level change projections, wave maxima change and GTSR data versus latitude, South America.

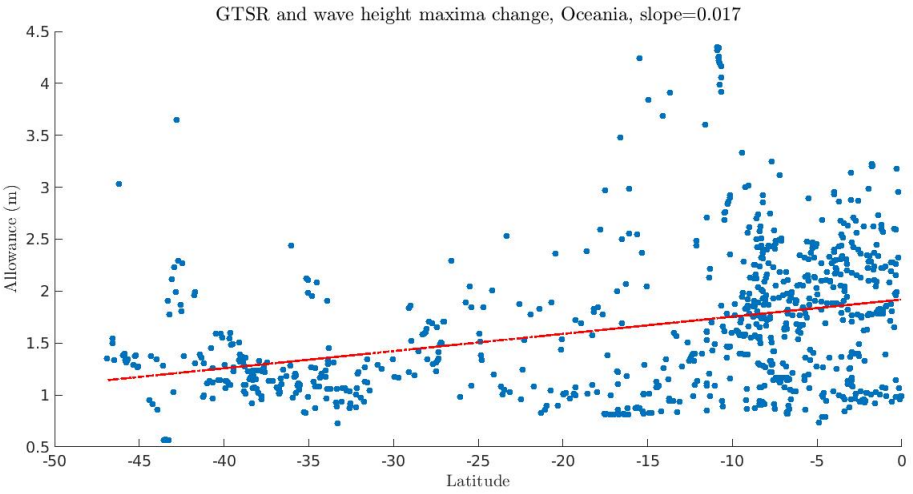


**Figure 5.10:** Allowances computed using sea level change projections, wave maxima change and GTSR data versus latitude, Oceania.

Asia (figure 5.12) has a significantly lower trend when including wave change by 0.004. Despite the increase of some points in Thailand and Indonesia, the large increase in large part of the Arctic Ocean, with the reduce of sea ice playing an important role in the increase of wave maxima at this area, as also the increase at the Sea of Japan and the East China Sea cause this drop in the trend. High increase in the equatorward trend is also observed for North America (Figure 5.11) and the

North Hemisphere part of Africa (Figure 5.13). For North America, the main reason is the absence of North Greenland high allowances due to the latitudinal limitation of the wave projections grid to 80 degrees. For North Africa the increase in trend is caused by the lower allowances observed in the Mediterranean combined with some higher allowances at the Gulf of Guinea.

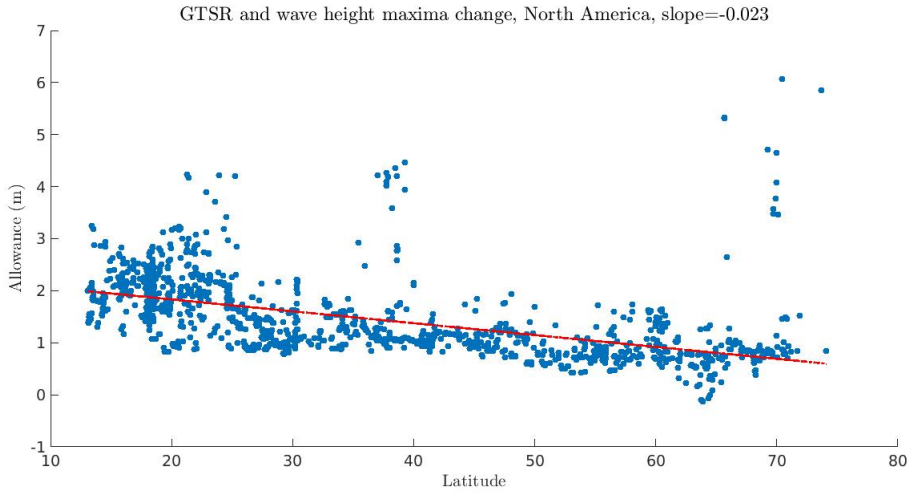


**Figure 5.11:** Allowances computed using sea level change projections, wave maxima change and GTSR data versus latitude, North America.

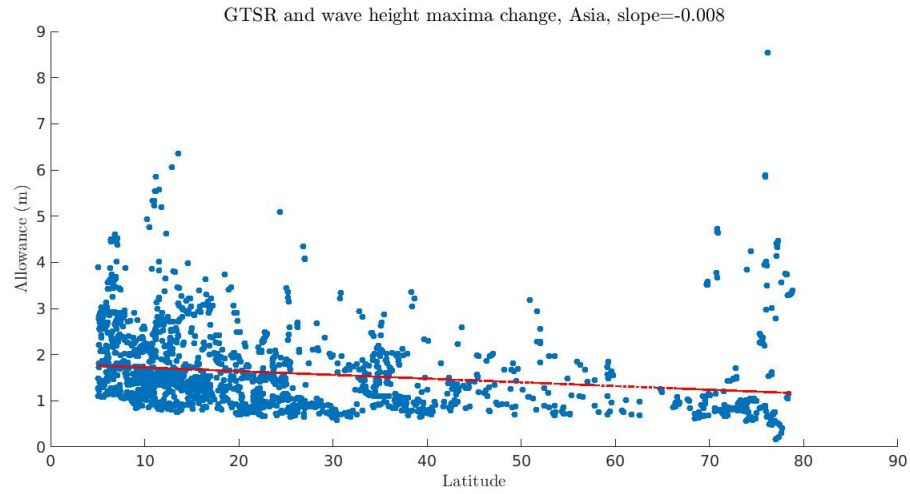


**Figure 5.12:** Allowances computed using sea level change projections, wave maxima change and GTSR data versus latitude, Asia.

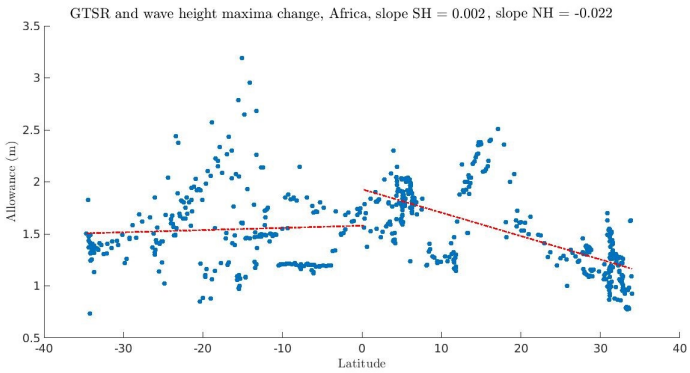


**Figure 5.13:** Allowances computed using sea level change projections, wave maxima change and GTSR data versus latitude, Africa.

It is now interesting to investigate to what extent these new allowances alter the exceedance frequencies in our grid.

### 5.2.3 Change in extreme events frequency

To quantify the effect of including the wave height maxima change from the historical period to the end of century, the percentages of points facing a severe change in extreme events frequency is computed. The computation is similar to the presented in subsection 2.3.4, using the new set of allowances including the change in wave maxima. The chosen investigated changes are also similar, thus a $10^3$ and a $10^4$ fold at the end of the century. As expected, the percentages of affected points are increasing with the contribution of wave maxima change. For $10^3$, $80.5\%$ of the grid points will be affected while for $10^4$ the percentage is $74.6\%$. Compared to the percentages for $10^3$ and $10^4$ without including wave data, the increase due to the wave maxima change is $2.4\%$ and $3.1\%$ respectively. Thus, the effect of wave maxima change will lead in more locations facing enormously higher frequencies of flooding events at the end of century, under the assumption that the present coastal structure will not change. Vousdoukas et al. (2017) used a different approach to compute the change in frequency of presently 1 per 100 years events for Europe in the end of century. Including the effect of relative Sea Level Change, tide and storm surges and waves, the computed European mean change is a 500 times fold.

### 5.2.4 Comparison of allowances at selected locations

We investigate again the nine selected tide gauge locations seen in subsection 3.1. For these locations the SLC probability distribution as well as the allowances computed using GESLA-2, GTSR, and GTSR including wave maxima change are plotted (Figure 5.14).

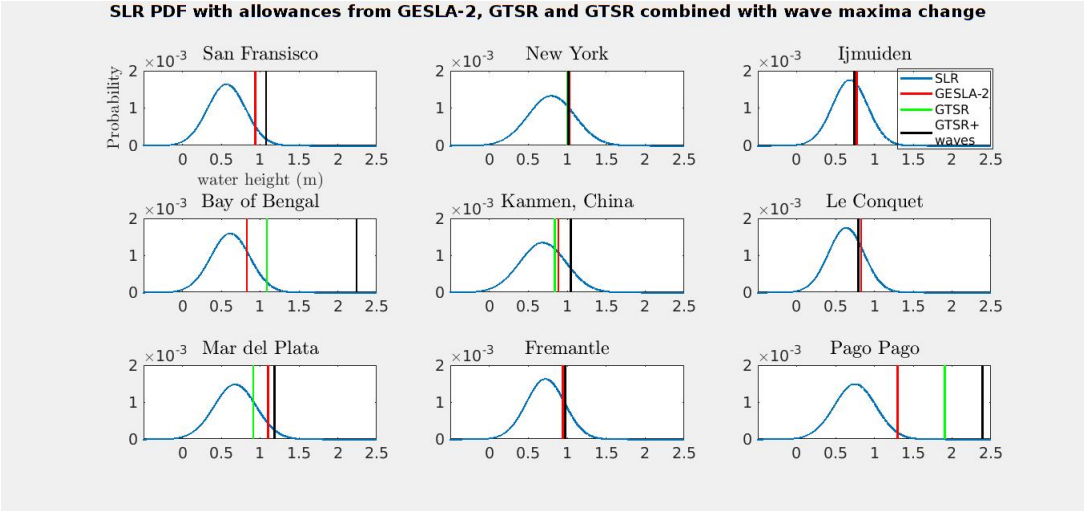


**Figure 5.14:** Sea Level Change PDF (blue curve) for nine specific locations, along with allowance using GESLA-2 (red), GTSR (green) and GTSR including wave height maxima change (black).

First, the underestimation of variability by GTSR is seen in the cases of Pago Pago, located in the West Pacific Ocean, and Bay of Bengal. In these areas, the allowances computed using GTSR are higher than the GESLA-2 ones by about 0.5 and 0.2 meters respectively. The rest of the locations are modeled well by GTSR, with an almost exact overlap in most cases. Allowances results are also in agreement with the scale parameters of the selected locations from Table reftablenine. Another observation is that especially for IJmuiden in The Netherlands, but also New York, Le Conquet in France and Fremantle in Southwest Australia, the height of allowances is very close to the mean sea level change and thus dominated by it. This is either due to low uncertainty in the Sea Level Change projections, or a high extreme water variability. This is not the case for San Francisco, where all allowances are about 0.5 m higher than the mean Sea Level Change.

Regarding waves, the effect is important in Pago Pago as including the change in maxima increases the allowance by about 0.5 m. In Mar del Plata and Kanmen wave change plays a smaller role, increasing the allowance by about 0.3 and 0.2 m respectively, due to the positive mode of the change distribution near Argentina and the high variability in both areas. Finally, the largest effect after including waves is observed in Bay of Bengal. As seen in subsection 5.1, North Indian Ocean shows both an increase in the peak of wave maxima and a high variability in the change distribution. These factors contribute in a domination of the allowance by waves effect than by the mean Sea Level Change.

Chapter 6

# Conclusion - Future Work

## 6.1 Conclusion

The GTSR dataset, used in this project to describe extreme waters variability, shows a good agreement with GESLA-2 at most locations. Though, in areas with low variability, or dominated by tropical cyclones there is a severe underestimation in the variability of extremes. At these areas, GESLA-2 Gumbel scale parameter can be up to more than 5 times larger than the GTSR one.

This underestimation leads to very high allowances of more than 2 meters at areas like the Caribbean as well as the Central and West Pacific Ocean. Moreover, because of the low variability within the Mediterranean, a contrast between South and North Europe allowances is observed. In general, allowances higher than 1 meter are computed for the largest part of the global coastline. The need for such increase in the height of coastal structure is reinforced by the fact that about $80\%$ of used points will face a multiplication in the frequency of exceedance events of up to 1000 times, and a slightly smaller percentage a multiplication of even up to 10000 times. These percentages grow about $3\%$ larger when the change in wave maxima between the historical period and the end of the century is included.

Taking in account the contribution of the change in wave maxima mostly affects remote islands in the Southern Ocean and the Bering Sea, but also other areas. The average contribution is an increase in the allowances. For Europe, the major factor of allowances increase due to waves change is the variability of the change distribution rather than the mean change. Allowances in areas like Pago Pago and Bay of Bengal appear to be dominated by the change in waves, while in other areas, like IJmuiden, mean Sea Level Change is the major factor adjusting the change in exceedance frequency.

To summarize, use of GTSR expanded the computation of allowances, giving satisfactory results for a large part of the global coastline. Thus, it creates a more clear picture of the effect of regional Sea Level Change, quantifying its role in flooding frequency more accurately. The attempt to include a new contribution in the allowances, the change in wave height maxima, shows that this effect cannot be neglected. In several locations it plays a large role in the change of the exceedance frequency and thus flooding safety. Finally, in both cases, positive allowance trends between 0.01 and 0.02 meters per degrees latitude are observed towards the equator, which are possibly because of the underestimation of extremes by the GTSR. Though, due to their consistency after including waves, the exact source of these trends is still to be determined.

## 6.2 Future Work

Several improvements can be made with an aim to gain a more accurate global set of allowances. In terms of extreme waters due to tide and storm surges, it is obvious that an improved meteorological grid able to resolve tropical cyclones and areas with low extremes variability will lead to computing correct allowances in areas that are now problematic and giving very high values. Moreover, it would be ideal to include more parameters, like waves, in the same model with tide and storm surges as also the non linear interactions between them which in GTSR are neglected.

In terms of Sea Level Change projections, the use of the upcoming CMIP6 models, as also improvements in bathymetry and ocean circulation, like adding incoming water by land ice and groundwater depletion into the flow, will hopefully lead to smaller uncertainty. Also, Slangen et al. (2017) showed that including different ice dynamics scenarios to the projections leads in important differences in the allowances. Thus, more research has to be done in ice dynamics, as determining the contribution in Sea Level Change can affect the results significantly.

Recent studies (Buchanan et al., 2016, 2017; Wahl et al., 2017) are working on improving the statistical framework on flooding, by using more detailed distributions like the Generalised Extreme Value and the Pareto distribution. Gumbel distribution is easy to handle and shows relatively good agreement with observations in many areas. GEV and Pareto though, bring several advantages like better describing the most unusual extremes and involving more data through using sub-annual maxima. Involving distributions with more parameters will lead to more accurate results in the area of flooding risk, but also specifically in the computation of allowances.

Finally, the concept of allowances as applied contains several assumptions. A revision and recalculation of allowances will have to take in account these assumptions and try to limit them. The most important one, is the assumption of constant variability. This may work well for some parameters, like tides, though it is probably far from an ideal assumption for others. A way to implement changes in variability would solve the problem of including parameters like wave change in a more delicate way. Secondly, the assumption that the change in exceedance frequency is dominated by the mean Sea Level Change also needs to be altered in order to obtain a more accurate set of allowances. That means the mean change of other contributions like extreme waters or waves has to be taken into account when computing an allowance. This is clear after the attempt to include the change in waves, of which the mean change is too large to be neglected, at least for specific areas like the Southern Ocean and the North Indian Ocean.

# Bibliography


Buchanan, M. K., Kopp, R. E., Oppenheimer, M., and Tebaldi, C. (2016). Allowances for evolving coastal flood risk under uncertain local sea-level rise. *Climatic Change*, 137(3-4):347–362.

Buchanan, M. K., Oppenheimer, M., and Kopp, R. E. (2017). Amplification of flood frequencies with local sea level rise and emerging flood regimes. *Environmental Research Letters*, 12(6).

Church, J. A., Clark, P. U., Cazenave, A., Gregory, J. M., Jevrejeva, S., Levermann, A., Merrifield, M. A., Milne, G. A., Nerem, R. S., Nunn, P. D., Payne, A. J., Pfeffer, W. T., Stammer, D., and Unnikrishnan, A. S. (2013). Sea level change. *Climate Change 2013: The Physical Science Basis. Contribution of Working Group I to the Fifth Assessment Report of the Intergovernmental Panel on Climate Change*, pages 1137–1216.

Hunter, J. R. (2012). A simple technique for estimating an allowance for uncertain sea-level rise. *Climatic Change*, 113(113).

Hunter, J. R., Church, J. A., White, N. J., and Zhang, X. (2013). Towards a global regionally varying allowance for sea-level rise. *Ocean Engineering*.

Hunter, J. R., Woodworth, P. L., Wahl, T., and Nicholls, R. J. (2017). Using global tide gauge data to validate and improve the representation of extreme sea levels in flood impact studies. *Global and Planetary Change*, 156:34–45.

Karnauskas, K. B., Lundquist, J. K., and Zhang, L. (2017). Southward shift of the global wind energy resource under high carbon dioxide emissions. *Nature Geoscience*, page 1.

Matthews, J. B. (2013). Ocean Surface Warming Part 1 : In situ measurement of the tropical Pacific top metre evaporation heat trap supports alpha / beta ocean global warming through asymmetric poleward heat transport and basal icemelt.

Menéndez, M. and Woodworth, P. L. (2010). Changes in extreme high water levels based on a quasi-global tide-gauge data set. *Journal of Geophysical Research: Oceans*, 115(10):1–15.

Muis, S., Verlaan, M., Winsemius, H. C., Aerts, J., and Ward, P. J. (2016). A global reanalysis of storm surges and extreme sea levels. *Nature Communications*, 7(June):11969.

Reerink, T. (2017). Seawise documentation. Technical report, Institute for Marine and Atmospheric research Utrecht.

Reerink, T. J., Kliphuis, M. A., and Van De Wal, R. S. W. (2010). Geoscientific Model Development Mapping technique of climate fields between GCM's and ice models. *Geosci. Model Dev*, 3:13–41.

Shepherd, A., Ivins, E. R., A, G., Barletta, V. R., Bentley, M. J., Bettadpur, S., Briggs, K. H., Bromwich, D. H., Forsberg, R., Galin, N., Horwath, M., Jacobs, S., Joughin, I., King, M. A., Lenaerts, J. T. M., Li, J., Ligtenberg, S. R. M., Luckman, A., Luthcke, S. B., McMillan, M., Meister, R., Milne, G., Mouginot, J., Muir, A., Nicolas, J. P., Paden, J., Payne, A. J., Pritchard, H., Rignot, E., Rott, H., Sørensen, L. S., Scambos, T. A., Scheuchl, B., Schrama, E. J. O., Smith, B., Sundal, A. V., van Angelen, J. H., van de Berg, W. J., van den Broeke, M. R., Vaughan, D. G., Velicogna, I., Wahr, J., Whitehouse, P. L., Wingham, D. J., Yi, D., Young, D., and Zwally, H. J. (2012). A reconciled estimate of ice-sheet mass balance. *Science*, 338(6111):1183–1189.

Slangen, A., van de Wal, R., Reerink, T., de Winter, R., Hunter, J. R., Woodworth, P., and Edwards, T. (2017). The Impact of Uncertainties in Ice Sheet Dynamics on Sea-Level Allowances at Tide Gauge Locations. *Journal of Marine Science and Engineering*, 5(2):21.

Slangen, A. B. A., Carson, M., Katsman, C. A., van de Wal, R. S. W., Köhl, A., Vermeersen, L. L. A., and Stammer, D. (2014). Projecting twenty-first century regional sea-level changes. *Climatic Change*, 124(1-2):317–332.

Vousdoukas, M. I., Mentaschi, L., Feyen, L., and Voukouvalas, E. (2017). Earth ' s Future Extreme sea levels on the rise along Europe ' s coasts Earth ' s Future. pages 1–20.

Wahl, T., Haigh, I. D., Nicholls, R. J., Arns, A., Dangendorf, S., Hinkel, J., and Slangen, A. B. A. (2017). Understanding extreme sea levels for broad-scale coastal impact and adaptation analysis. *Nature Communications*, 8(May):1–12.

Wang, X. L., Feng, Y., and Swail, V. R. (2014). Changes in global ocean wave heights as projected using multimodel CMIP5 simulations. *Geophysical Research Letters*, 41(3):1026–1034.

Woodworth, P. L., Hunter, J. R., Marcos, M., Caldwell, P., Men Endez, M., and Haigh, I. (2017). Towards a global higher-frequency sea level dataset. *Geosci. Data J*, 3:50–59.

# Appendix

## A SeaWISE

Quoted from the documentation of the SeaWISE program (Reerink, 2017):

"The composed distribution $P(x)$ consists for each $x$ of all contributions of two independent distributions $P_1(x_1)$ and $P_2(x_2)$ for which the summed $x$-axis values $x_1$ and $x_2$ add to $x$. So each combination for which applies $x = x_1 + x_2$ yields a contribution of $P_1(x_1)\ P_2(x_2)$ to $P(x)$. $P(x)$ is determined by looping over all relevant combinations $x = x_1 + x_2$:

$$P(x) = \sum_{m=c}^{d} P_1(x - m\Delta_x)P_2(m\Delta_x) \tag{A.1}$$

where $x$ is the sealevel rise (SLR) and $P_1$ and $P_2$ are the probability distributions for SLR of two individual components, which are supposed to be independent here.

With the $n$-sigma interval we will refer to the interval between the left and right $n$-sigma boundaries of a distribution centered around its mode. The mode is the $x$ value that corresponds with the peak value of $P(x)$. We often will take $n$=5, which means that about $99.9\%$ of the integrated distribution lies within this interval. We also normalize the distribution on this $n$-sigma interval.

Selecting the SLR data within $n$-sigma (e.g. $99.9\%$ with $n$=5) of the integrated distribution around the mode, defines for each probability distribution a left and right $n$-sigma boundary. Suppose we have a part of the $x$-axis divided in $n$ intervals of $\Delta_x$. The interval counter $m$ runs between $c$ and $d$ corresponding with $x_c$ and $x_d$ the left and right boundaries of $P_2$, while taking $x_1 = x - m\Delta_x$ and $x_2 = m\Delta_x$.

To obtain the entire distribution $P(x)$ A.1 is calculated from $x_a$ the left $n$-sigma boundary of $P_1$ up to $x_b$ + $x_d$ or to $n$, where $x_b$ is the right $n$-sigma boundary of $P_1$. "

## B Gumbel fit with MATLAB

In order to fit a Gumbel distribution to the obtained significant wave height data, MATLAB evfit command was used. Evfit receives as input an array, in this case the annual maxima of historical and end century significant wave height data, and gives as output the location and scale parameters of Gumbel distribution. To test the results, computation was made also with the package ismev of the language R, giving similar results. These two ways of fitting a Gumbel distribution were also tested by Hunter et al. (2017) showing good agreement.

## C Wave Projections check

For the 8 CMIP5 models used (Table 2.1), Gumbel distributions were fitted in order to check whether a similar pattern occurs. In order to check the behavior of all models a Gumbel fit was made for each model, seen in Figures C.1-C.4. Results show indeed a similar pattern, with differences in

the magnitude and varability of the maxima. There are two clear high wave areas at high latitudes with location parameters of more than 10 meters. These areas also present higher variability, with scale parameters reaching values around 2. Closer to the equator both location and scale parameters are lower, meaning lower wave heights and smaller variability. In terms of magnitude, CNRM-CM5 stands out presenting lower values in all cases, with location parameters barely reaching 10 meters and the scale parameters 1.5 in the high wave areas. On the other hand, MIROC-5 and MRI-CGCM3 have the highest location and scale parameters for both periods with location parameters going above 15 meters and scale parameters reaching 2.5. From Figures C.1-C.4 no solid conclusion on the change between the two time periods can be extracted.

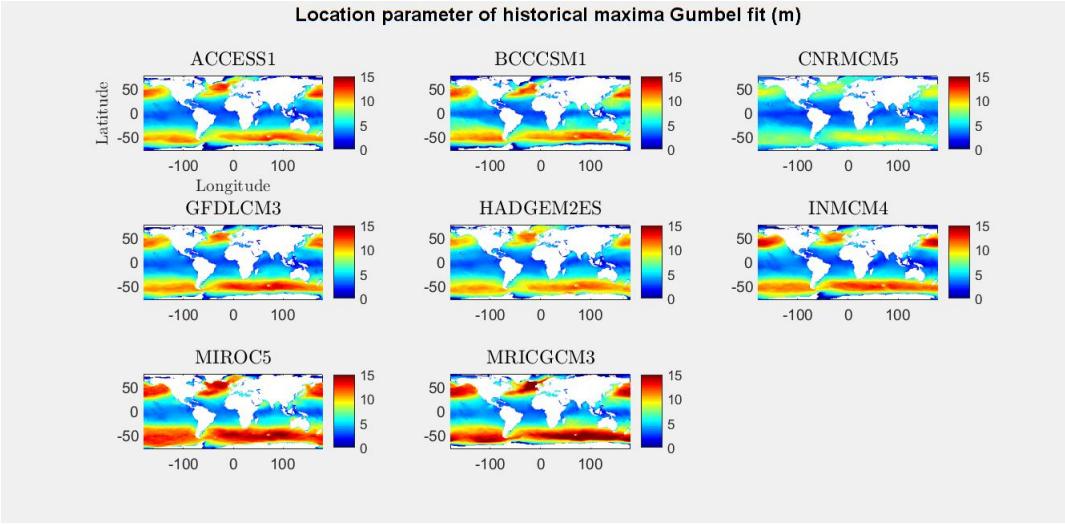


**Figure C.1:** Location parameter from historical maxima Gumbel fit for all models.

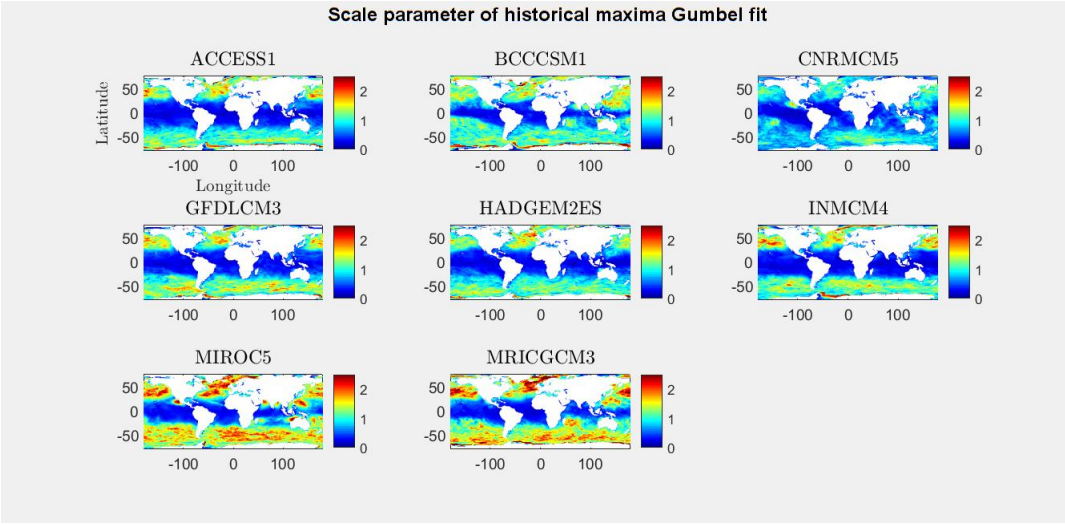


**Figure C.2:** Scale parameter from historical maxima Gumbel fit for all models.

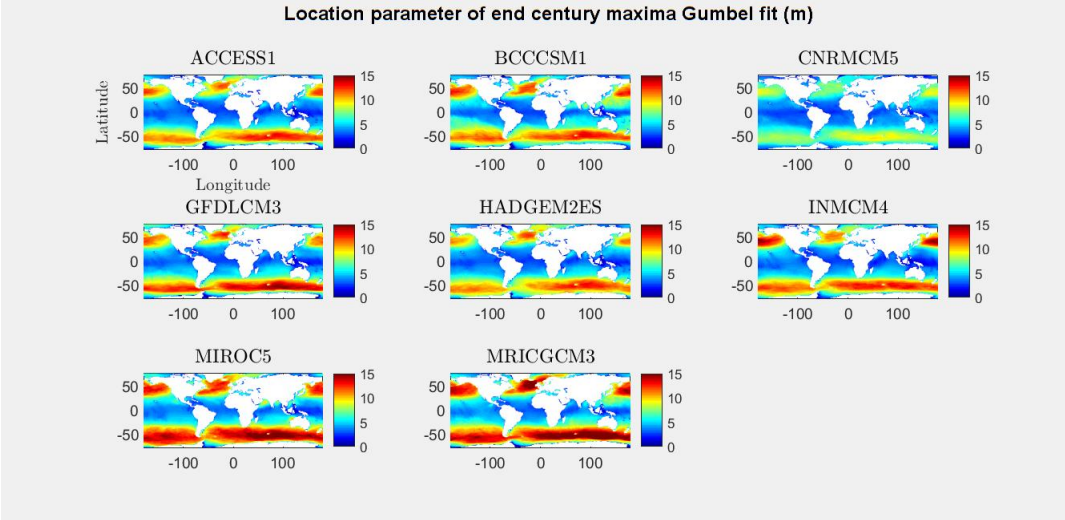


**Figure C.3:** Location parameter from end century maxima Gumbel fit for all models.

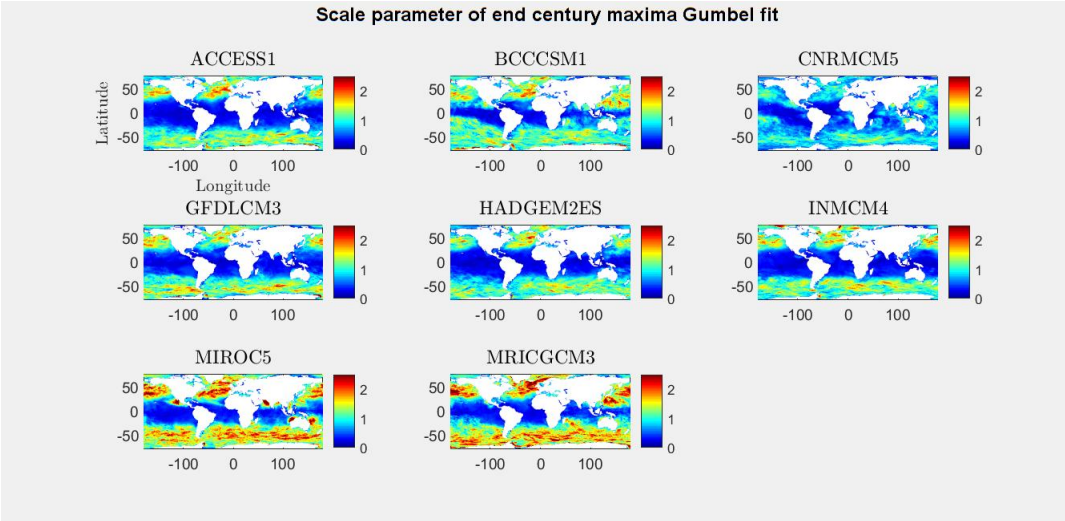


**Figure C.4:** Scale parameter from end century maxima Gumbel fit for all models.